Cancer Cell International

RESEARCH

Open Access

CCDC110 promotes the progression of hepatocellular carcinoma by activating the TGF-β/SMAD signaling pathway through targeted regulation of TGFBR1

Hao Shen[1*], Haifeng Li[2] and Haodong Tang[2]

Abstract

Background Hepatocellular carcinoma (HCC) is recognized for its high growth rate, high degree of invasiveness, and tendency to spread, leading to a significant number of deaths. In the course of studying the transcriptome of HCC tissues, the protein coiled-coil domain-containing 110 (CCDC110) was identified. By employing tandem mass tag (TMT) quantitative proteomics, this research identified transforming growth factor beta receptor 1 (TGFBR1) as a potential target influenced by CCDC110. The purpose of this study was to examine the role of CCDC110 in the growth and invasion of HCC and to identify new potential targets for the treatment of HCC.

Methods In vitro and in vivo experiments were conducted to investigate the role and mechanism of CCDC110 in promoting the malignant behaviors of hepatocellular carcinoma through the regulation of TGFBR1.

Results We determined that the mRNA and protein levels of CCDC110 are elevated in hepatocellular carcinoma tissues and cell lines, which is correlated with a worse patient prognosis. CCDC110 enhances the proliferation of hepatocellular carcinoma cells, reduces their apoptosis, and increases their migration and invasion capabilities. In the cytoplasm, CCDC110 interacts with TGFBR1, enhancing stability of TGFBR1, promoting proliferation, and reducing the apoptosis, migration, and invasion of hepatocellular carcinoma cells through TGFBR1 both in vivo and in vitro. The CCDC110-TGFBR1 axis stimulates EMT, thereby enhancing the malignant biological behavior of hepatocellular carcinoma by activating the TGF-β/SMAD signaling pathway. The protein levels of CCDC110/TGFBR1 in hepatocellular carcinoma tissues are highly expressed and positively correlated. A combined analysis of CCDC110 and TGFBR1 provides improved guidance for the prognosis of patients with hepatocellular carcinoma.

Conclusion CCDC110 is highly expressed in hepatocellular carcinoma tissues and cell lines, and the CCDC110-TGFBR1 axis facilitates EMT and the malignant biological behavior of hepatocellular carcinoma through the activation of the TGF-β/SMAD signaling pathway.

Keywords CCDC110, TGFBR1, Hepatocellular carcinoma, Proliferation, Metastasis, EMT

*Correspondence:
Hao Shen
1976354009@qq.com
[1] Department of Thyroid Breast Surgery, Shanghai East Hospital, School of Medicine, Tongji University, Shanghai 200120, China
[2] Department of Hepatic-Biliary-Pancreatic Center, Zhongda Hospital, Medical School, Southeast University, Nanjing 210000, China

Introduction

Hepatocellular carcinoma (HCC) is a highly proliferative, invasive, and metastatic malignant tumor with a high mortality rate, and it represents the most common (over 80%) pathological type of primary liver cancer [1, 2]. In China, HCC accounts for 9.0% of all new malignant tumor cases, ranking fifth, and accounts for 13.0% of all

© The Author(s) 2025. **Open Access** This article is licensed under a Creative Commons Attribution-NonCommercial-NoDerivatives 4.0 International License, which permits any non-commercial use, sharing, distribution and reproduction in any medium or format, as long as you give appropriate credit to the original author(s) and the source, provide a link to the Creative Commons licence, and indicate if you modified the licensed material. You do not have permission under this licence to share adapted material derived from this article or parts of it. The images or other third party material in this article are included in the article's Creative Commons licence, unless indicated otherwise in a credit line to the material. If material is not included in the article's Creative Commons licence and your intended use is not permitted by statutory regulation or exceeds the permitted use, you will need to obtain permission directly from the copyright holder. To view a copy of this licence, visit http://creativecommons.org/licenses/by-nc-nd/4.0/.

malignant tumor deaths, making it the second leading cause of cancer death [3–5]. The majority of HCC cases (about 65%) are linked to hepatitis B virus infection, with other types of viral hepatitis, aflatoxin exposure, and non-alcoholic fatty liver disease also serving as risk factors [6–9]. Despite treatment options such as surgical resection or liver transplantation, the risk of recurrence or metastasis remains high, leading to a poor prognosis for HCC patients [1, 10, 11]. Although numerous genetic and epigenetic studies on HCC have been conducted, significant breakthroughs in understanding the mechanisms of HCC proliferation and metastasis are still needed. Therefore, further research into HCC is necessary to discover new biological markers, explore new therapeutic targets, and develop personalized treatment strategies for HCC patients.

Coiled-coil domain-containing proteins feature coiled-coil structural domains, which are highly conserved superhelical domains composed of α-helical peptides that wrap around each other [12].About 10% of proteins in biological organisms contain coiled-coil domains, which are among the simplest and most widespread domains facilitating protein–protein interactions [13, 14]. The CCDC protein family is expressed in numerous tissues, with diverse subcellular localizations, allowing them to participate in a wide range of physiological processes [15]. At the cellular level, they are involved in chromosome separation, DNA recognition and cleavage, and the promotion of interactions between various proteins [15]. Several CCDC proteins have been found to be abnormally expressed in different tumor tissues, including those of gastric and colorectal cancers [16–23], and some have been implicated in regulating tumor cell proliferation, invasion, and metastasis [20, 24, 25].

Coiled-coil domain-containing protein 110 (CCDC110), a member of the coiled-coil domain-containing protein family, is located on chromosome 4 and contains coiled-coil structural domains similar to those of other family members. Research has identified CCDC110 as a promising target for cancer diagnosis and treatment [26–30]. The internal region of CCDC110 includes a leucine zipper (ZIP) motif, which is composed of leucine repeat sequences (L1, L2, L3, L4, and L5) separated by six amino acid residues, followed by basic residues, characteristic of proteins with ZIP motifs [31]. This motif also enables multiple protein–protein interactions [27]. qRT-PCR analysis of various tumor samples and cancer cell lines revealed elevated mRNA levels of CCDC110 in several cancer types, including tongue, gastric, melanoma, and hepatocellular carcinoma [26]. However, the role of CCDC110 in hepatocellular carcinoma has not been fully explored, prompting this study to investigate CCDC110 expression in hepatocellular carcinoma tissues and cell lines, as well as its impact and mechanisms on cell proliferation, apoptosis, invasion, and migration.

TGFBR1 acts as a receptor for transforming growth factor beta (TGF-β), a pivotal molecule in the TGF-β signaling pathway [32, 33]. The activation of this pathway can initiate epithelial-mesenchymal transition (EMT) [33–35], a process in which epithelial cells acquire a mesenchymal phenotype, markedly increasing cell motility. This transition is essential for tumor metastasis [35–37]. Furthermore, activation of the TGF-β signaling pathway promotes EMT, malignant transformation, and angiogenesis, contributing to tumor progression [37–39]. Previous research has revealed the overexpression of TGFBR1 in various malignancies, with its dysregulated expression interfering with cellular processes and facilitating tumor development and progression [40–43].

The cellular functions of humans rely significantly on protein interactions, which are crucial in various biological processes, including cell signaling, cell cycle regulation, intercellular communication, and metabolism [44–46]. Research indicates that protein interactions can generate new binding sites, influencing the expression of other genes and creating a dynamic cellular system. A disruption in this balance may lead to a range of diseases, including cancer.

To date, the interaction between CCDC110 and TGFBR1 has not been explored. The results of the present study suggest that CCDC110 is highly expressed in hepatocellular carcinoma tissues and cell lines, and the CCDC110-TGFBR1 axis facilitates EMT and the malignant biological behavior of hepatocellular carcinoma through the activation of the TGF-β/SMAD signaling pathway.

Methods

1. Bioinformatics analysis

The HCC transcriptome data and clinical information were downloaded from the TCGA (https://portal.gdc.cancer.gov/) database. R software (version 3.6.1) was used to conduct specific analyses.

2. Clinical samples and cell cultures

In total, 100 pairs of HCC tissues and matched adjacent normal tissues were collected from Zhongda Hospital affiliated with Southeast University. Our study was approved by the Ethical Committee of Zhongda Hospital affiliated with Southeast University for the use of tissue samples for research purposes. Informed consent was obtained from all of the patients. All HCC specimens were staged

according to the 2020 AJCC HCC staging system. The HCC patients with higher and lower CCDC110 expression levels than the median were allocated to the high- and low-expression groups, respectively, as shown in Table 2.

The human HCC cell lines YY8103, MHCC97-L, Huh7, and HCCLM3 and the human normal liver cell line THLE-2 were purchased from the Chinese Academy of Science. All the cell lines were cultured at 37 °C in a humidified chamber with 5% CO2. All culture media contained 10% fetal bovine serum (FBS; Gibco).

3. Quantitative real-time PCR (qRT-PCR)

Total RNA was extracted from HCC cells and tumor tissues via TRIzol reagent (Invitrogen). The RNA quality and concentration were analyzed via a Nanodrop 2000. The extracted RNA was reverse transcribed to cDNA using TransScript® II First-Strand cDNA Synthesis SuperMix (TransGen). qRT-PCR was then performed using SYBR Green PCR Master Mix (Yeasen). The primers used are listed in Supplementary Table 4.

4. Cellular lentivirus transfection

To generate stably transfected cell lines, CCDC110, RO60, ELMOD2, WNT5A, FNBP1L, TGFBR1 and shCCDC110, shRO60, shELMOD2, shWNT5A, shFNBP1L, and shTGFBR1 lentiviral vectors were purchased from Guangzhou Yijin Biotechnology Company.

5. Western blotting and Co-IP

The collected cells were lysed in a solution containing RIPA lysis buffer containing phosphatase inhibitors and protease inhibitors (Beyotime, China). BCA reagent (Beyotime, China) was used to measure protein concentrations. Commensurable amounts of protein were separated via SDS-PAGE, transferred to a membrane, and incubated with various antibodies. Finally, the data were acquired via Image Lab 5.2.1. The antibodies used were as follows: CCDC110, RO60, ELMOD2, WNT5A, FNBP1L, TGFBR1, Bcl-2, Bax, caspase-3, cleaved-caspase-3, smad2, p-smad2, smad3, p-smad3, MMP2, MMP9, E-cadherin, N-cadherin, vimentin and GAPDH. All of these antibodies, except for CCDC110, which was purchased from LifeSpan BioSciences, were purchased from Abcam. For the Co-IP assay, the beads were preincubated with the appropriate antibody. Next, we lysed the cells with Co-IP buffer. After centrifugation, the supernatant was incubated with the beads at 4 °C overnight. Finally, we washed the beads, added SDS buffer, and determined the immunoprecipitates by western blot.

6. Immunohistochemistry and Immunofluorescence

Surgical samples were fixed in 4% paraformaldehyde. All the sections were routinely deparaffinized, rehydrated through an alcohol series, and subjected to antigen retrieval with citrate antigen retrieval solution (Beyotime). The sections were blocked with 5% normal goat serum with 0.1% Triton X-100 and 3% H2O2 in PBS for 1 h at room temperature, incubated with appropriate primary antibodies at 4 °C overnight, and then incubated with secondary antibodies. IHC staining was finally detected via light microscopy (Nikon, Tokyo, Japan). For immunofluorescence analysis, the cells were cultured on poly-d-lysine-coated cover slides (Sigma, Germany). The cells were washed twice with PBS, fixed in 4% formaldehyde for 15 min and then permeabilized with 0.5% Triton X-100/PBS for 15 min at room temperature. The permeabilized cells were blocked with 10% donkey serum albumin for 1 h. Immunostaining was performed by incubation with the corresponding primary antibodies overnight at 4 °C. The next day, the cells were washed with PBS and then incubated with Alexa Fluor 555-conjugated secondary antibodies (Beyotime) for 1 h at 37 °C. Finally, the cells were treated with 2-(4-amidinophenyl)–6-indolecarbamidine dihydrochloride (Beyotime). Fluorescence images were obtained using fluorescence microscopy (Leica Microsystems Imaging Solutions, Cambridge, UK).

7. Cell proliferation, cell migration and invasion, and cell apoptosis assays

For the Cell Counting Kit-8 (CCK-8, Dojindo Laboratories, Japan) assay, the cells were seeded into 96-well plates in triplicate. The cell viability was measured according to the manufacturer's protocol. For the colony formation assay, the cells were seeded into 6-well plates (500 cells/well) in triplicate and cultured for 10 days. The colonies were fixed, stained and counted. For the EdU assay kit (RiboBio, China), the cells were seeded into 24-well plates (3×10^4 cells/well) in triplicate. After being cultured for 24 h, the cells were incubated with 50 μM EdU for 2 h. Subsequent staining and visualization were carried out following the manufacturer's instructions. The ratio of EdU-positive cells to total cells was calculated and analyzed in three random fields. Transwell inserts (Corning) with or without Matrigel (BD Biosciences) were utilized to perform migration and invasion assays according to the manufacturer's protocol. The migrated/invaded cells were photographed and counted with a light microscope. For the apoptosis assay, the Annexin V-FITC/PI Apoptosis Detection Kit (Key-

GEN, China) was used to stain the cells according to the manufacturer's manual. The percentage of apoptotic cells was determined via flow cytometry.

8. Transcriptome sequencing and tandem mass tag (TMT) quantitative proteomics technology.

After 6 pairs of fresh hepatocellular carcinoma tissue samples were collected at this center, subsequent transcriptome sequencing and analysis were performed at Shanghai Jikai Gene Medical Technology Co., Ltd. After CCDC110 was knocked down in HCCLM3 cells and the knockdown efficiency was verified via western blotting, the CCDC110-knockdown cell group and the control group (three samples in each group) were sent to Shanghai Jikai Gene Medical Technology Co., Ltd., for TMT-based quantitative proteomics analysis.

9. Protein stability experiment

After MHCC97-L LV-NC cells were cultured and MHCC97-L LV-CCDC110 cells were transfected in a 6-well plate, 2 μL of 50 mg/mL cycloheximide (CHX) was added to the first well of the 6-well plate, the mixture was gently shaken, and regular culture was continued. Every two hours, we added to each well until all the wells contained cycloheximide. After the last well of cycloheximide was added, the cells in the 6-well plate were subjected to total protein extraction via the same method as before. After protein extraction, the supernatant was collected for subsequent electrophoresis detection.

10. Animal models and IHC

For the subcutaneous tumor growth model, 4-week-old male BALB/c nude mice were utilized. A total of 5×10^6 transfected cells were subcutaneously injected into the right side of each mouse. Tumor size was measured weekly. The following formula was used to calculate the tumor volume: Volume = Length × Width2 × 0.5. We euthanized all the mice after 5 weeks. Then, the tumors were collected, weighed, and subjected to IHC staining. For the tail vein metastasis model, 1×10^6 transfected cells were injected into the tail vein of nude mice. The metastases were visualized via an IVIS Spectrum in vivo imaging system. Finally, all the mice were sacrificed after 8 weeks. Lung tissues were collected and further analyzed via H&E staining. For IHC, the retrieved tissues were fixed, embedded and sectioned. We incubated the slides with primary antibody at 4 °C overnight, followed by incubation with secondary antibody for 1 h at room temperature. We used 3,3'-diaminobenzidine (DAB) and hematoxylin to stain the slides. Eventually, three random fields on each slide were acquired for analysis.

For the orthotopic models, tumors from the aforementioned subcutaneous HCC models were minced into 1–2 mm^3 cubes and transplanted into the livers of BALB/c mice. Four weeks after transplantation, MRI was performed, and the mice were euthanized.

11. Construction of a hepatocellular carcinoma tissue organoid model

HCC tissue organoid models were established as described in our previous study using fresh tumor tissues from patients with HCC. Photographs of the HCC tissue organoids were taken daily. Tissue organoids were transfected with shCCDC110, LV-CCDC110, or the corresponding control lentivirus. HCC tissue organoids were harvested after incubation for 10 days in Matrigel.

12. Statistical analysis

SPSS 26.0 software was used to perform the statistical analysis of the experimental data we obtained, and the final data are presented as the mean ± standard deviation (X ± SD). Independent sample t-tests were used for two groups of metric data, paired sample t-tests were used for analyzing paired samples, analysis of variance was used for comparisons between multiple groups, the Kaplan–Meier method was used for prognosis analysis of clinical samples, the chi-square test was used for analyzing count data in clinical correlation analysis, and linear regression was used for expression correlation analysis. A p-value < 0.05 was considered to indicate statistical significance ($p<0.05$ is marked as *$p<0.01$ is marked as **$p<0.001$ is marked as ***).

Results

Expression levels of CCDC110 in HCC tissues and cell lines.

The initial step involved differential expression analysis of the transcriptome sequencing data, revealing that, compared with their corresponding normal tissues, 1019 genes were significantly upregulated in hepatocellular carcinoma tumor tissues ($p<0.05$, log2FoldChange > 1). By prioritizing genes based on their p values, the nine genes with the most significant differences in expression were identified: ROBO1, GPC3, NPAS2, TOP2A, CCDC110, E2F1, CENPF, TCF19, and PEG10. Excluding those genes previously reported to be associated with the malignant biology of hepatocellular carcinoma cells, CCDC110 was chosen for further investigation (Figure S1) (Table 1). Subsequent analysis of data from the TCGA database confirmed that CCDC110 expression was significantly elevated in hepatocellular carcinoma tumor

Table 1 Differential expression analysis of transcriptome sequencing results in hepatocellular carcinoma tissue

Gene name	T	N	log2FoldChange	pvalue	padj
ROBO1	845.6484143	124.6869553	2.760530301	2.09E−35	4.24E−31
GPC3	5417.319106	43.96382847	6.947382713	1.01E−15	1.02E−12
NPAS2	221.6863523	47.56890053	2.225465233	6.03E−15	4.69E−12
TOP2A	629.5900452	25.85637569	4.604278964	2.53E−14	1.65E−11
CCDC110	1729.706442	478.4573625	1.854205632	3.30E−14	2.09E−11
E2F1	117.7392615	10.17712585	3.540882432	3.65E−14	2.17E−11
CENPF	208.9560115	12.60883928	4.046139881	5.35E−14	3.01E−11
TCF19	181.3485639	32.08423309	2.500233347	1.11E−13	5.93E−11
PEG10	9537.647657	89.11599997	6.742828333	1.47E−13	7.44E−11

(See figure on next page.)

Fig. 1 Expression levels of CCDC110 in hepatocellular carcinoma tissue and cell lines, and its relationship with prognosis of hepatocellular carcinoma patients. **A** Analysis of CCDC110 expression levels in hepatocellular carcinoma tissue ($n = 371$) and normal liver tissue ($n = 50$) in the TCGA database. **B** Kaplan–Meier analysis in the TCGA database showing the overall survival of hepatocellular carcinoma patients with different levels of CCDC110 expression. **C** qRT-PCR detection of CCDC110 expression in 100 pairs of hepatocellular carcinoma tumor tissue and their paired normal liver tissue. **D** Western blot experiment to detect the protein expression of CCDC110 in 8 pairs of randomly selected hepatocellular carcinoma tumor tissue and their paired normal liver tissue. **E** qRT-PCR analysis of CCDC110 expression levels in four hepatocellular carcinoma cell lines and normal liver cells. **F** Western blot experiment to detect the protein expression of CCDC110 in four hepatocellular carcinoma cell lines and normal liver cells. **G** Immunohistochemical staining and scoring of CCDC110 in hepatocellular carcinoma tissue (Scale bar: 100 μm, 50 μm). **H** Kaplan–Meier analysis showing the overall survival of 100 hepatocellular carcinoma patients collected from this center with different levels of CCDC110 expression. (***$p < 0.001$, **$p < 0.01$, *$p < 0.05$)

tissues compared with normal liver tissues ($p < 0.01$) (Fig. 1A). Additionally, survival analysis indicated that patients with higher CCDC110 expression levels had poorer prognoses ($p < 0.001$) (Fig. 1B).

To corroborate the findings from the TCGA database, qRT-PCR was used to assess the expression level of CCDC110 in tumor tissues and matched normal liver tissues from 100 hepatocellular carcinoma patients. This analysis revealed a significant increase in the mRNA expression level of CCDC110 in hepatocellular carcinoma tumor tissues ($p < 0.001$) (Fig. 1C). Furthermore, eight pairs of tumor tissue samples and corresponding normal liver tissue samples from HCC patients were randomly selected for western blot experiments. These experiments confirmed that the protein expression level of CCDC110 was significantly greater in hepatocellular carcinoma tumor tissues than in matched normal tissues (Fig. 1D). In addition, we selected four hepatocellular carcinoma cell lines (Huh7, YY8103, HCCLM3, and MHCC97-L) and a normal liver cell line (THLE-2) for qRT-PCR and western blot experiments, and the results revealed that the expression levels of CCDC110 mRNA and protein were significantly greater in hepatocellular carcinoma cell lines than in normal liver cells ($p < 0.05$) (Fig. 1E, F). Furthermore, immunohistochemical staining revealed that the expression of CCDC110 was significantly greater in hepatocellular carcinoma tumor tissues than in normal liver tissues (Fig. 1G). To further study the relationship between CCDC110 expression levels and the clinicopathological features of hepatocellular carcinoma patients, we divided 100 hepatocellular carcinoma patients into a high-expression group ($n = 50$) and a low-expression group ($n = 50$) according to the median expression level of CCDC110. The expression level of CCDC110 was significantly positively correlated with various clinical parameters of hepatocellular carcinoma tumors, including size, number, envelope integrity, microvascular invasion, Edmondson stage, and TNM stage ($p < 0.05$) (Table 2). In addition, Kaplan–Meier survival analysis revealed that patients with high CCDC110 expression had shorter overall survival ($p < 0.01$, Hazard Ratio = 2.273, 95% CI of ratio:1.310 to 3.945) (Fig. 1H). These experimental results suggest that CCDC110 is highly expressed in both hepatocellular carcinoma tissues and cell lines and is associated with poor prognosis in hepatocellular carcinoma patients.

CCDC110 can promote the proliferation, invasion, and migration of hepatocellular carcinoma cells while inhibiting apoptosis

Previous experiments have shown that, compared with normal liver cells (THLE-2), CCDC110 is highly expressed in four hepatocellular carcinoma cell lines. An analysis of four hepatocellular carcinoma cell

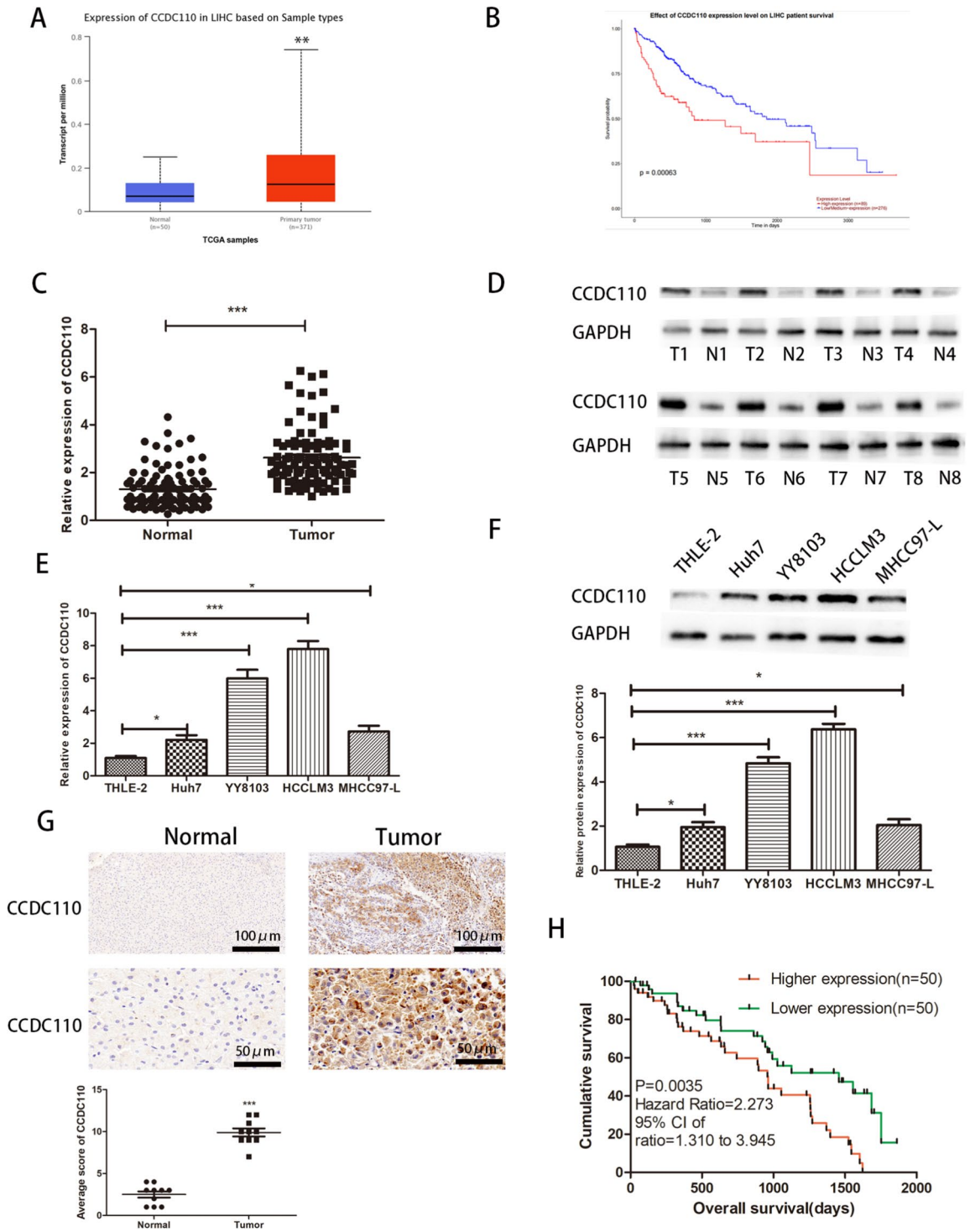

Fig. 1 (See legend on previous page.)

lines revealed that CCDC110 was relatively highly expressed in the HCCLM3 and YY8103 cell lines, whereas its expression levels were relatively low in the Huh7 and MHCC97-L cell lines. Therefore, we constructed CCDC110-knockdown cell lines (HCCLM3 and YY8103) and CCDC110-overexpressing cell lines (Huh7 and MHCC97-L), and the transfection efficiency of each cell line was validated via qRT-PCR. The results revealed that sh-CCDC110-3 (sh3) had the best

Table 2 The relationship between CCDC110 expression level and clinical pathological features of hepatocellular carcinoma patients (n = 100)

Characteristics	Number	CCDC110expression level		P值
		Low expression group(n = 50)	high expression group(n = 50)	
Age				
< 50	29	16	13	0.508
≥ 50	71	34	37	
Gender				
Male	49	23	26	0.548
Female	51	27	24	
Cirrhosis status				
Yes	83	40	43	0.424
No	17	10	7	
HBs Antigen				
Yes	83	42	41	0.790
No	17	8	9	
Tumor size(cm)				
< 5	47	36	11	< 0.001***
≥ 5	53	14	39	
Microvascular invasion				
Yes	44	15	29	0.005**
No	56	35	21	
Number of tumors				
Single	62	42	20	< 0.001***
Multiple	38	8	30	
AFP(ng/ml)				
≤ 20	54	28	26	0.688
> 20	46	22	24	
Edmonson stage				
I–II	53	32	21	0.027*
III–IV	47	18	29	
Tumor capsule integrity				
Complete	43	28	15	0.008**
Incomplete	57	22	35	
TNM stage				
I	48	31	17	0.005**
II–III	52	19	33	

* p < 0.05, ** p < 0.01, *** p < 0.001

knockdown efficiency, and the overexpression virus also had a high overexpression efficiency (p < 0.001) (Figure S2).

According to the results of the CCK-8 assay, knocking down CCDC110 significantly inhibited the proliferative activity of hepatocellular carcinoma cells (HCCLM3, YY8103) (p < 0.001) (Fig. 2A). However, overexpressing CCDC110 significantly promoted the proliferation of hepatocellular carcinoma cells (Huh7 and MHCC97-L cells) (p < 0.01) (Fig. 3A). A colony formation assay revealed that knocking down CCDC110 significantly inhibited the colony formation ability of hepatocellular carcinoma cells (HCCLM3, YY8103) (p < 0.01) (Fig. 2B), while overexpressing CCDC110 significantly promoted the colony formation ability of hepatocellular carcinoma cells (Huh7 and MHCC97-L cells) (p < 0.01) (Fig. 3B). Similarly, the results of the EdU incorporation assay revealed that knocking down CCDC110 significantly decreased the percentage of EdU-positive hepatocellular carcinoma cells (HCCLM3, YY8103) (p < 0.01) (Fig. 2C), while overexpressing CCDC110 significantly increased the percentage of EdU-positive hepatocellular carcinoma cells (Huh7 and MHCC97-L) (p < 0.01) (Fig. 3C). These results indicate that CCDC110 can promote the proliferation of hepatocellular carcinoma cells.

Transwell assays revealed that knocking down CCDC110 significantly reduced the migration and invasion ability of hepatocellular carcinoma cells (HCCLM3, YY8103) (p < 0.01) (Fig. 2D, E), while overexpressing CCDC110 significantly promoted the migration and invasion ability of hepatocellular carcinoma cells (MHCC97-L and Huh7 cells) (p < 0.05) (Fig. 3D, E). The experimental results indicate that CCDC110 promotes the migration and invasion of hepatocellular carcinoma cells.

CCDC110 expression in HCC tissue organoids further validated the in vitro functional results. Compared with the control, CCDC110 knockdown and overexpression resulted in significantly decreased and increased HCC tissue organoid diameters, respectively (Figs. 2F, 3F).

Next, we conducted apoptosis experiments and found that after the knockdown of CCDC110 in HCCLM3 and YY8103 cells, cell apoptosis significantly increased (p < 0.001) (Fig. 4A, B), while overexpressing CCDC110 in Huh7 and MHCC97-L cells significantly reduced cell apoptosis (p < 0.01) (Fig. 4C, D). This study revealed that CCDC110 inhibits the apoptosis of hepatocellular carcinoma cells.

The results of this series of functional experiments indicate that CCDC110 can enhance the malignant biological behavior of hepatocellular carcinoma cells.

Using TMT to screen downstream target proteins of CCDC110

To determine which differentially expressed proteins can serve as potential target proteins for CCDC110, we used TMT-based quantitative proteomics technology to

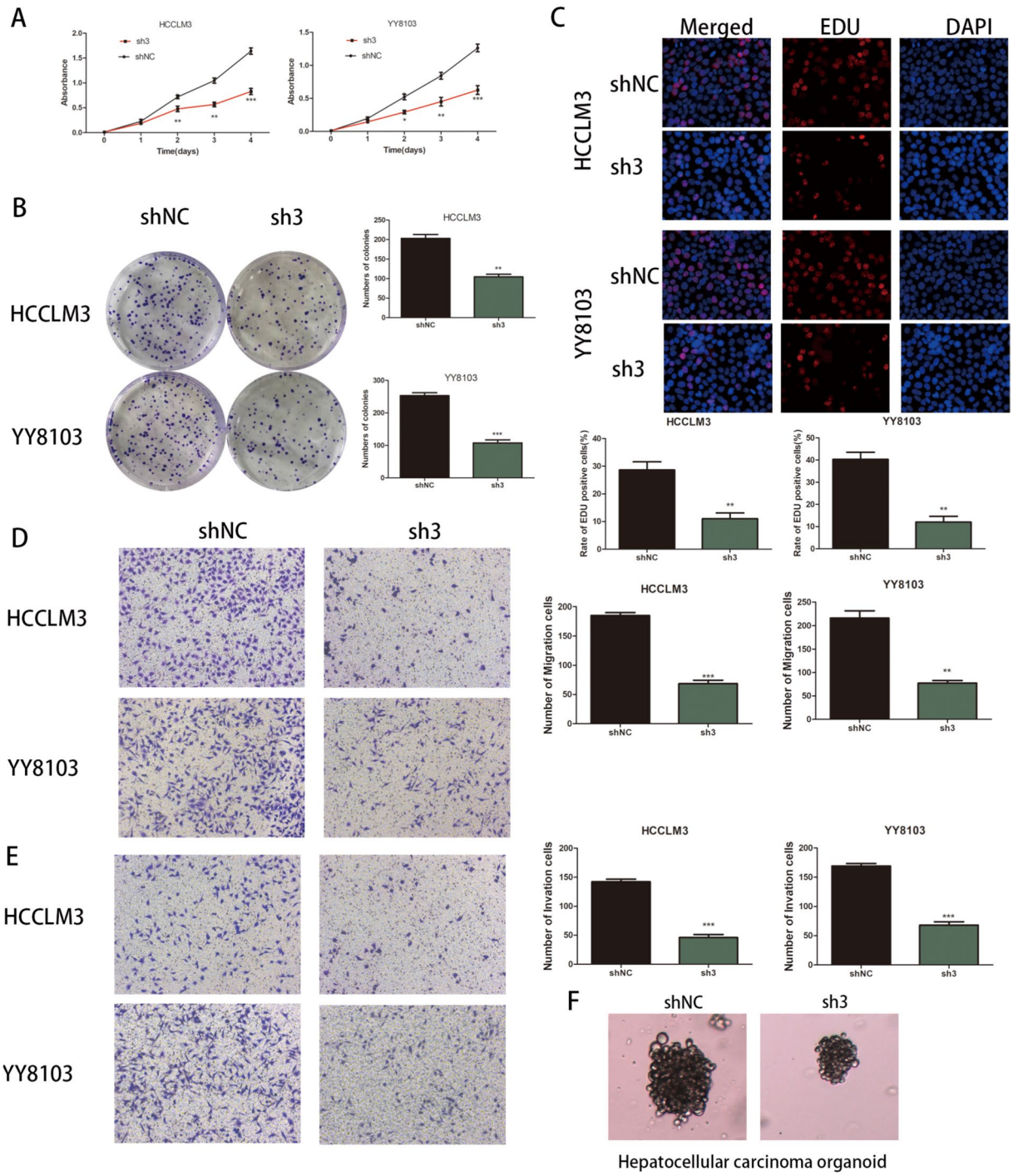

Fig. 2 Downregulation of CCDC110 expression reduces the proliferation, migration, and invasion ability of hepatocellular carcinoma cell lines in vitro. **A** Knockdown of CCDC110 in HCCLM3 and YY8103 cell lines and CCK-8 assay was performed with control group cells; **B** Knockdown of CCDC110 in HCCLM3 and YY8103 cell lines and plate colony formation experiment was performed with control group cells; **C** Knockdown of CCDC110 in HCCLM3 and YY8103 cell lines and EdU experiment was performed with control group cells (scale bar, 50 μm); **D**, **E** Knockdown of CCDC110 in HCCLM3 and YY8103 cell lines and cell migration and invasion experiments were performed with control group cells (scale bar, 50 μm). **F** Light field images of HCC tissue organoids after CCDC110 knockdown mediated by lentivirus infection, or control lentivirus(scale bar, 100 μm).(***$p < 0.001$, **$p < 0.01$)

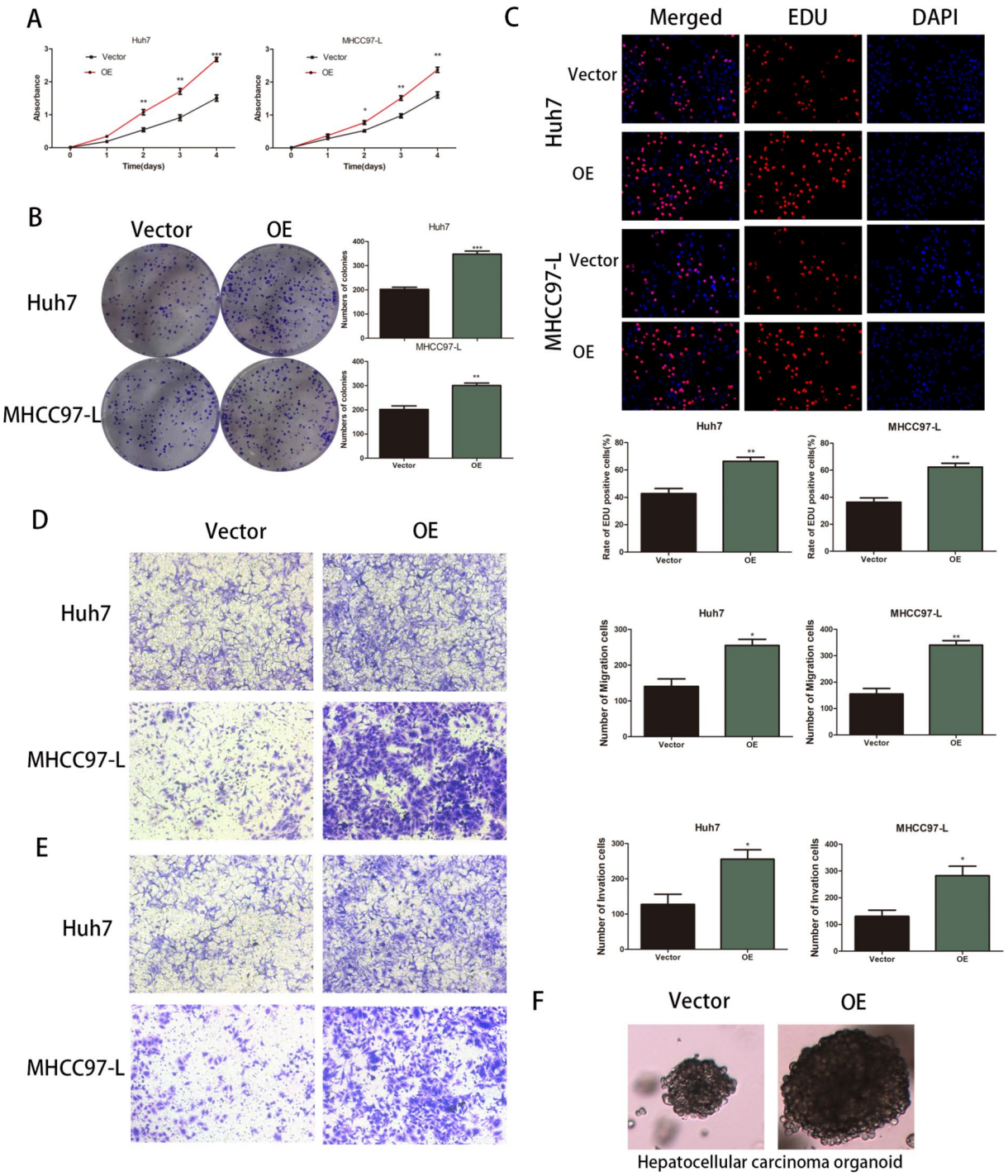

Fig. 3 Upregulation of CCDC110 expression promotes the proliferation, migration, and invasion ability of hepatocellular carcinoma cell lines in vitro. **A** Overexpression of CCDC110 in Huh7 and MHCC97-L cell lines and CCK-8 assay was performed with control group cells; **B** Overexpression of CCDC110 in Huh7 and MHCC97-L cell lines and plate colony formation experiment was performed with control group cells; **C** Overexpression of CCDC110 in Huh7 and MHCC97-L cell lines and EdU experiment was performed with control group cells (scale bar, 100 μm); **D**, **E** Overexpression of CCDC110 in Huh7 and MHCC97-L cell lines and cell migration and invasion experiments were performed with control group cells (scale bar, 50 μm). **F** Light field images of HCC tissue organoids after CCDC110 overexpression mediated by lentivirus infection, or control lentivirus(scale bar, 100 μm).(***$p < 0.001$, **$p < 0.01$, *$p < 0.05$)

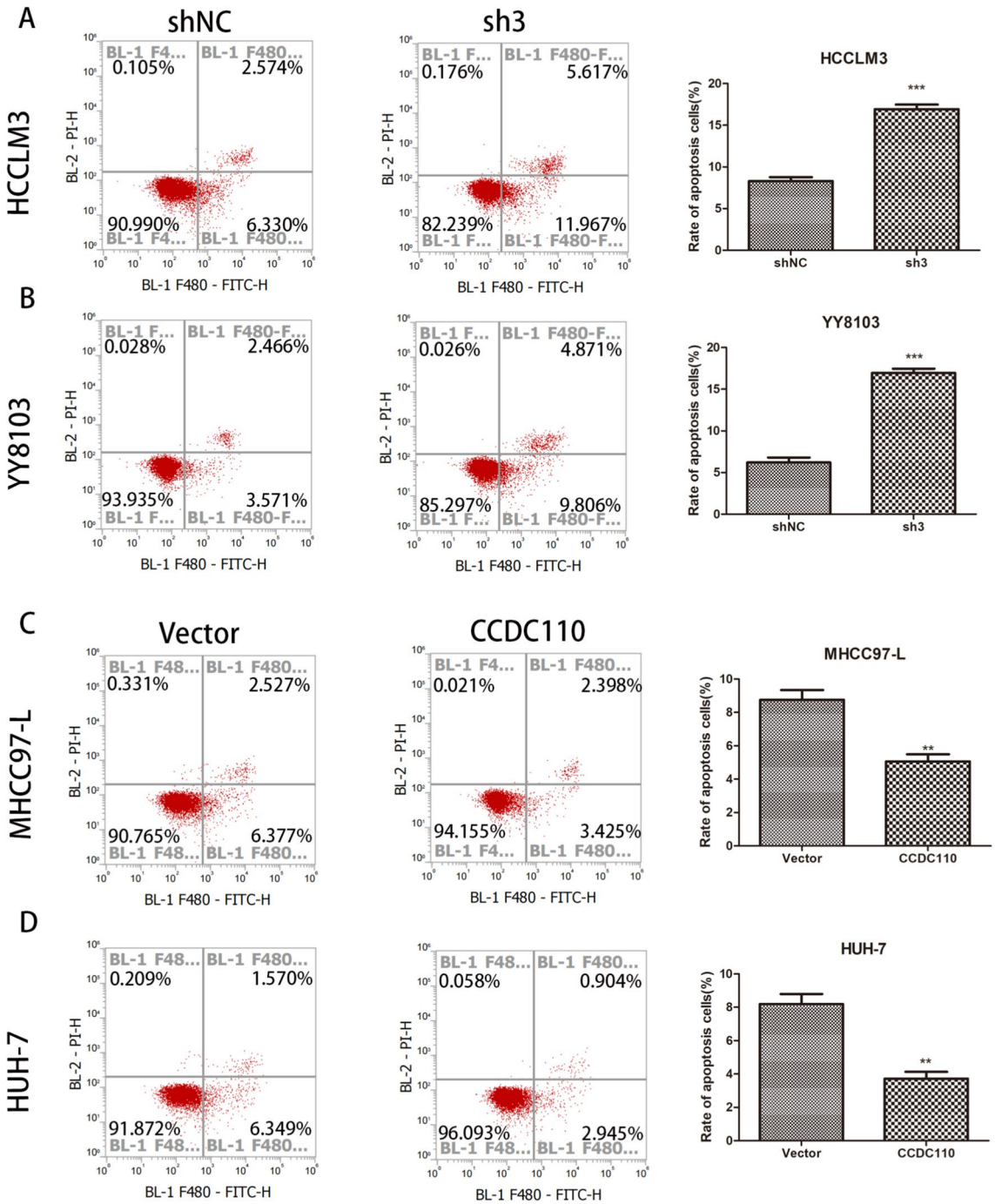

Fig. 4 The effect of CCDC110 on the apoptosis ability of hepatocellular carcinoma cell lines. **A**, **B** Knockdown of CCDC110 in HCCLM3 and YY8103 cell lines and apoptosis detection were performed with control group cells; **C**, **D**. Overexpression of CCDC110 in Huh7 and MHCC97-L cell lines and apoptosis detection were performed with control group cells. (***p < 0.001, **p < 0.01)

analyze the total protein content of HCCLM3 cells stably expressing sh-CCDC110 or sh-NC. A total of 7,679 proteins were identified for further quantitative analysis. Compared with those in the control group, there were 158 downregulated proteins (Table 3) and 87 upregulated proteins in HCCLM3 cells with CCDC110 knockdown. Among the downregulated proteins, we selected the five proteins most closely related to CCDC110 based on p values (RO60, ELMOD2, WNT5A, TGFBR1, and FNBP1L).

Table 3 Proteins downregulated in the CCDC110 knockdown group as identified by TMT screening

Accession	GeneName	Molecular Weight[kDa]	ShRNA/NC	Regulation	P value
P10155	RO60	60.6	0.814882033	DOWN	1.7735E−06
Q8IZ81	ELMOD2	34.9	0.812990937	DOWN	2.08081E−05
P41221	WNT5A	42.3	0.75	DOWN	3.33025E−05
P36897	TGFBR1	55.9	0.695111613	DOWN	7.10915E−05
Q5T0N5	FNBP1L	70	0.733603005	DOWN	8.12482E−05
O75844	ZMPSTE24	54.8	0.806441902	DOWN	0.000206855
Q8N4J0	CARNMT1	47.2	0.719403841	DOWN	0.000207084
Q9UQR0	SCML2	77.2	0.71114913	DOWN	0.000226672
Q9BZF1	OSBPL8	101.1	0.818181818	DOWN	0.000232621
P25445	FAS	37.7	0.729316806	DOWN	0.000247446
O75083	WDR1	66.2	0.711840228	DOWN	0.000259147
O94888	UBXN7	54.8	0.711637193	DOWN	0.000282777
P48029	SLC6A8	70.5	0.705999431	DOWN	0.000321683
O75122	CLASP2	141	0.785480512	DOWN	0.000358782
P53794	SLC5A3	79.6	0.811594203	DOWN	0.000431032
Q13951	CBFB	21.5	0.759824047	DOWN	0.000435606
Q9NPI6	DCP1A	63.2	0.754165449	DOWN	0.000587995
Q9Y3Q3	TMED3	24.8	0.786777844	DOWN	0.000616541
Q10472	GALNT1	64.2	0.793185894	DOWN	0.000665935
P11021	HSPA5	72.3	0.71477565	DOWN	0.000809696
Q8WWI1	LMO7	192.6	0.774918663	DOWN	0.000810212
Q9UPP1	PHF8	117.8	0.746942341	DOWN	0.000860432
Q96K37	SLC35E1	44.7	0.817933959	DOWN	0.000920529
P32754	HPD	44.9	0.666388889	DOWN	0.000992063
Q13884	SNTB1	58	0.76056338	DOWN	0.001049924
O60669	SLC16A7	52.2	0.735106998	DOWN	0.001062853
Q9BRQ6	CHCHD6	26.4	0.764705882	DOWN	0.001262121
Q9BZC7	ABCA2	269.7	0.659933592	DOWN	0.001298232
A6NHR9	SMCHD1	226.2	0.670843776	DOWN	0.00133753
O43237	DYNC1LI2	54.1	0.774327122	DOWN	0.001354949
Q9NUJ3	TCP11L1	57	0.808863431	DOWN	0.001367685
Q969Q6	PPP2R3C	53.3	0.832875038	DOWN	0.001380905
O60331	PIP5K1C	73.2	0.769094662	DOWN	0.001418798
Q9Y239	NOD1	107.6	0.502003005	DOWN	0.001653451
O75718	CRTAP	46.5	0.825068451	DOWN	0.001695886
Q2T9J0	TYSND1	59.3	0.810745548	DOWN	0.00180355
Q9Y5J5	PHLDA3	13.9	0.809710495	DOWN	0.001853728
P10114	RAP2A	20.6	0.796407186	DOWN	0.001991403
P13674	P4HA1	61	0.828153565	DOWN	0.002075964
P04083	ANXA1	38.7	0.662233306	DOWN	0.00219935
Q8N2H3	PYROXD2	63	0.752848379	DOWN	0.002218506
P49247	RPIA	33.2	0.812688822	DOWN	0.00222317
Q14643	ITPR1	313.7	0.769389561	DOWN	0.002371574
Q08499	PDE4D	91.1	0.75314052	DOWN	0.00242117
Q96HY7	DHTKD1	103	0.734894478	DOWN	0.00242934
O00462	MANBA	100.8	0.833180568	DOWN	0.002826474
Q9P206	KIAA1522	107	0.809954751	DOWN	0.002846719
P18669	PGAM1	28.8	0.779359431	DOWN	0.00284699
P20700	LMNB1	66.4	0.828153565	DOWN	0.002929361

Table 3 (continued)

Accession	GeneName	Molecular Weight[kDa]	ShRNA/NC	Regulation	P value
Q12955	ANK3	480.1	0.550387597	DOWN	0.002995548
O43314	PPIP5K2	140.3	0.823404255	DOWN	0.003131946
Q9H1U4	MEGF9	62.9	0.811047389	DOWN	0.003171165
Q00534	CDK6	36.9	0.7809439	DOWN	0.003240376
Q9BYT8	NLN	80.6	0.815128593	DOWN	0.003263686
O60513	B4GALT4	40	0.735106998	DOWN	0.003347138
Q96RY7	IFT140	165.1	0.67879127	DOWN	0.003559349
Q9UPM8	AP4E1	127.2	0.802343046	DOWN	0.003628254
Q92930	RAB8B	23.6	0.799579958	DOWN	0.003684266
Q8NHP6	MOSPD2	59.7	0.736903039	DOWN	0.003814814
Q08752	PPID	40.7	0.760856808	DOWN	0.003844554
P61077	UBE2D3	16.7	0.819284415	DOWN	0.003925096
Q9BX63	BRIP1	140.8	0.581334036	DOWN	0.003926167
Q9H2X9	SLC12A5	126.1	0.597444089	DOWN	0.004128994
Q32P28	P3H1	83.3	0.805597352	DOWN	0.004257184
Q9HB21	PLEKHA1	45.5	0.813236627	DOWN	0.004301073
Q9NQW1	SEC31B	128.6	0.554404145	DOWN	0.004469309
A6NJ78	METTL15	46.1	0.806985848	DOWN	0.004577054
Q02410	APBA1	92.8	0.558556219	DOWN	0.004780581
O75781	PALM	42.1	0.792650134	DOWN	0.004782483
Q96SW2	CRBN	50.5	0.770433756	DOWN	0.004831558
Q9NX38	ABITRAM	20.4	0.792650134	DOWN	0.005157823
Q13233	MAP3K1	164.4	0.748761294	DOWN	0.005330305
P15848	ARSB	59.6	0.746724891	DOWN	0.005334474
P05186	ALPL	57.3	0.650165017	DOWN	0.005352942
Q16890	TPD52L1	22.4	0.830131138	DOWN	0.005608247
Q7L5Y1	ENOSF1	49.8	0.744186047	DOWN	0.005626871
Q96I76	GPATCH3	59.3	0.555209953	DOWN	0.00577333
Q8WZ42	TTN	3813.7	0.648351648	DOWN	0.005819972
P05187	ALPP	57.9	0.735106998	DOWN	0.006140819
Q9H3K2	GHITM	37.2	0.774852071	DOWN	0.006667043
Q8N0Z3	SPICE1	96.2	0.794258373	DOWN	0.006776183
B7ZAP0	RABGAP1L	29	0.745925495	DOWN	0.006924955
Q3L8U1	CHD9	325.8	0.823404255	DOWN	0.006946199
Q10471	GALNT2	64.7	0.829216224	DOWN	0.007154275
O75460	ERN1	109.7	0.775147929	DOWN	0.007295848
O75204	TMEM127	25.8	0.794795094	DOWN	0.00742099
Q8NBP0	TTC13	96.8	0.738626485	DOWN	0.00748874
Q15283	RASA2	96.6	0.627951153	DOWN	0.008173751
Q92738	USP6NL	94	0.807228916	DOWN	0.008507301
O75251	NDUFS7	23.5	0.79395933	DOWN	0.008699526
P31327	CPS1	164.8	0.830384381	DOWN	0.008979692
Q03135	CAV1	20.5	0.82038835	DOWN	0.00953711
P09923	ALPI	56.8	0.759824047	DOWN	0.00984423
P56962	STX17	33.4	0.828153565	DOWN	0.009951334
Q9Y2G8	DNAJC16	90.5	0.786543614	DOWN	0.010348657
Q9ULW6	NAP1L2	52.5	0.46092038	DOWN	0.010417066
P00533	EGFR	134.2	0.788375559	DOWN	0.010497774
Q5VUA4	ZNF318	251	0.828710759	DOWN	0.010795979

Table 3 (continued)

Accession	GeneName	Molecular Weight[kDa]	ShRNA/NC	Regulation	P value
Q02535	ID3	13	0.767078916	DOWN	0.011272985
Q96JA4	MS4A14	76.5	0.543209877	DOWN	0.011368508
Q99743	NPAS2	91.7	0.798022176	DOWN	0.011663326
Q9NYP7	ELOVL5	35.3	0.758499414	DOWN	0.01187371
Q05481	ZNF91	137.1	0.71624714	DOWN	0.011913328
Q5T4B2	CERCAM	67.5	0.645010965	DOWN	0.012651543
Q14005	IL16	141.7	0.693480102	DOWN	0.014985491
P50416	CPT1A	88.3	0.738626485	DOWN	0.015050005
Q53LP3	SOWAHC	55.6	0.821190043	DOWN	0.015465343
Q8WUD1	RAB2B	24.2	0.791579576	DOWN	0.015867918
Q969L2	MAL2	19.1	0.821743091	DOWN	0.015875817
P35580	MYH10	228.9	0.523616049	DOWN	0.016278633
P32004	L1CAM	139.9	0.814333233	DOWN	0.016296327
P62745	RHOB	22.1	0.783888228	DOWN	0.016357964
Q9H3H5	DPAGT1	46.1	0.746942341	DOWN	0.016659352
Q96AG3	SLC25A46	46.1	0.794557416	DOWN	0.017001982
O75901	RASSF9	50	0.475405804	DOWN	0.017069846
Q9Y6N5	SQOR	49.9	0.820940819	DOWN	0.017336673
Q13686	ALKBH1	43.8	0.821493625	DOWN	0.017342763
Q15018	ABRAXAS2	46.9	0.739849188	DOWN	0.017895847
Q92570	NR4A3	68.2	0.78412132	DOWN	0.018223881
Q6NUK4	REEP3	29.2	0.796706587	DOWN	0.018556149
P48067	SLC6A9	78.2	0.760046935	DOWN	0.018862666
O00458	IFRD1	50.2	0.793185894	DOWN	0.019937977
P39210	MPV17	19.7	0.803968731	DOWN	0.019995817
Q9P2X0	DPM3	10.1	0.824262694	DOWN	0.020224803
Q9NV35	NUDT15	18.6	0.832061069	DOWN	0.02040244
Q6ZN66	GBP6	72.4	0.584940555	DOWN	0.020535584
P11182	DBT	53.5	0.810500905	DOWN	0.020572198
Q86UY8	NT5DC3	63.4	0.811594203	DOWN	0.020946561
Q9Y244	POMP	15.8	0.765450265	DOWN	0.022759598
Q8NBM4	UBAC2	38.9	0.811047389	DOWN	0.025569456
P31260	HOXA10	42.4	0.79181601	DOWN	0.025684242
Q9H7C4	SYNC	55.3	0.829015544	DOWN	0.02624468
O43739	CYTH3	46.3	0.792114695	DOWN	0.026611964
P15941	MUC1	122	0.806140879	DOWN	0.028003692
Q9Y3Y4	PYGO1	45.1	0.832620648	DOWN	0.028021508
Q9UMX5	NENF	18.8	0.828405974	DOWN	0.028742035
P19075	TSPAN8	26	0.789976134	DOWN	0.029343653
P02511	CRYAB	20.1	0.744186047	DOWN	0.029712863
Q9ULG6	CCPG1	87.3	0.811839323	DOWN	0.030413629
Q15047	SETDB1	143.1	0.81677771	DOWN	0.031026716
Q6P1L8	MRPL14	15.9	0.777547393	DOWN	0.031125447
Q8WW43	APH1B	28.4	0.811047389	DOWN	0.0315503
P48775	TDO2	47.8	0.584786054	DOWN	0.032725486
Q9NX14	NDUFB11	17.3	0.819836215	DOWN	0.033686683
Q8TBB1	LNX1	80.6	0.682837914	DOWN	0.034223492
Q53FT3	HIKESHI	21.6	0.80481203	DOWN	0.035408662
Q66K89	E4F1	83.4	0.742160279	DOWN	0.036810059

Table 3 (continued)

Accession	GeneName	Molecular Weight[kDa]	ShRNA/NC	Regulation	P value
Q9NZP5	OR5AC2	35.3	0.487357462	DOWN	0.037307351
O14681	EI24	38.9	0.789206917	DOWN	0.038092873
Q96GC6	ZNF274	74.1	0.756440281	DOWN	0.039881463
Q9Y5F0	PCDHB13	87.5	0.685008422	DOWN	0.040009557
Q9H8M2	BRD9	67	0.82537268	DOWN	0.040033256
P54851	EMP2	19.2	0.825068451	DOWN	0.041504789
Q7Z7A3	CTU1	36.4	0.750583431	DOWN	0.041806925
O75381	PEX14	41.2	0.761303582	DOWN	0.045096106
P28827	PTPRM	163.6	0.798321846	DOWN	0.045687728
Q5JU69	TOR2A	35.7	0.793484758	DOWN	0.047291713
Q96J66	ABCC11	154.2	0.778535428	DOWN	0.048658301

The CCDC110-TGFBR1 axis promotes the proliferation, migration, and invasion ability of hepatocellular carcinoma cells in vitro

Western blot analysis of the expression of RO60, ELMOD2, WNT5A, TGFBR1, and FNBP1L in HCCLM3 cells with CCDC110 knockdown. After the knockdown of CCDC110, the expression levels of RO60, WNT5A, and TGFBR1 in HCCLM3 cells were significantly reduced, whereas the expression levels of ELMOD2 and FNBP1L did not significantly change (Figure S3A). Subsequent functional recovery experiments revealed that overexpressing RO60 and WNT5A in CCDC110-knockdown HCCLM3 cells did not significantly affect the inhibition of cell proliferation and migration caused by CCDC110 knockdown (Figure S3B-D). However, overexpressing TGFBR1 in CCDC110-knockdown HCCLM3 cells significantly enhanced the malignant biological behavior of the cells inhibited by CCDC110 knockdown ($p < 0.01$) (Fig. 5A–D). Similarly, Western blot experiments detected the expression of RO60, ELMOD2, WNT5A, TGFBR1, and FNBP1L in MHCC97-L cells overexpressing CCDC110. After overexpressing CCDC110, the expression levels of RO60, WNT5A, and TGFBR1 in MHCC97-L cells significantly increased, whereas the expression levels of ELMOD2 and FNBP1L did not significantly change (Figure S4A). Knocking down RO60 and WNT5A in CCDC110-overexpressing MHCC97-L cells did not significantly change the enhanced cell proliferation, migration, or invasion caused by CCDC110 overexpression (Figure S4B–D). However, overexpressing TGFBR1 in CCDC110-overexpressing MHCC97-L cells significantly inhibited the enhanced cell proliferation, migration, and invasion caused by CCDC110 overexpression ($p < 0.01$) (Fig. 5A–D). Therefore, TGFBR1 may be a potential target of CCDC110. CCDC110 promotes the malignant biological behavior of liver cancer cells through TGFBR1.

To further investigate the interaction between CCDC110 and TGFBR1, qRT-PCR and Western blot experiments were initially conducted to assess the expression levels of TGFBR1 in HCCLM3 cells with CCDC110 knockdown and in MHCC97-L cells with CCDC110 overexpression. The findings indicated that TGFBR1 expression levels were decreased in HCCLM3 cells following CCDC110 knockdown, whereas TGFBR1 expression levels were increased in MHCC97-L cells upon CCDC110 overexpression (Fig. 6A, B). Exogenous immunoprecipitation (Co-IP) experiments were subsequently performed by transfecting equal amounts of the Flag-CCDC110 plasmid and HA-TGFBR1 plasmid into HCCLM3 and MHCC97-L cells. We found that in HCC cells, coimmunoprecipitation (IP) with Flag-labeled CCDC110 coprecipitated with HA-labeled TGFBR1. Similarly, immunoprecipitation of HA-labeled TGFBR1 via coprecipitation with Flag-labeled CCDC110 was detected (Fig. 6C). The endogenous Co-IP experiment also revealed that immunoprecipitation with the CCDC110 antibody coprecipitated with TGFBR1, whereas immunoprecipitation with the TGFBR1 antibody coprecipitated with CCDC110 (Fig. 6D). Moreover, we observed the localization of CCDC110 and TGFBR1 in hepatocellular carcinoma cells using laser confocal microscopy. Subcellular localization analysis revealed that CCDC110 was predominantly located in the cytoplasm of hepatocellular carcinoma cells, and TGFBR1 was also found in the cytoplasm of these cells. The presence of overlapping fluorescence signals confirmed that CCDC110 and TGFBR1 colocalized in the cytoplasm of hepatocellular carcinoma cells (Fig. 6E), laying the foundation for their interaction.

The above experiments demonstrated that knocking down CCDC110 can downregulate the expression of TGFBR1 and that CCDC110 can interact with TGFBR1. Therefore, we performed a CHX half-life

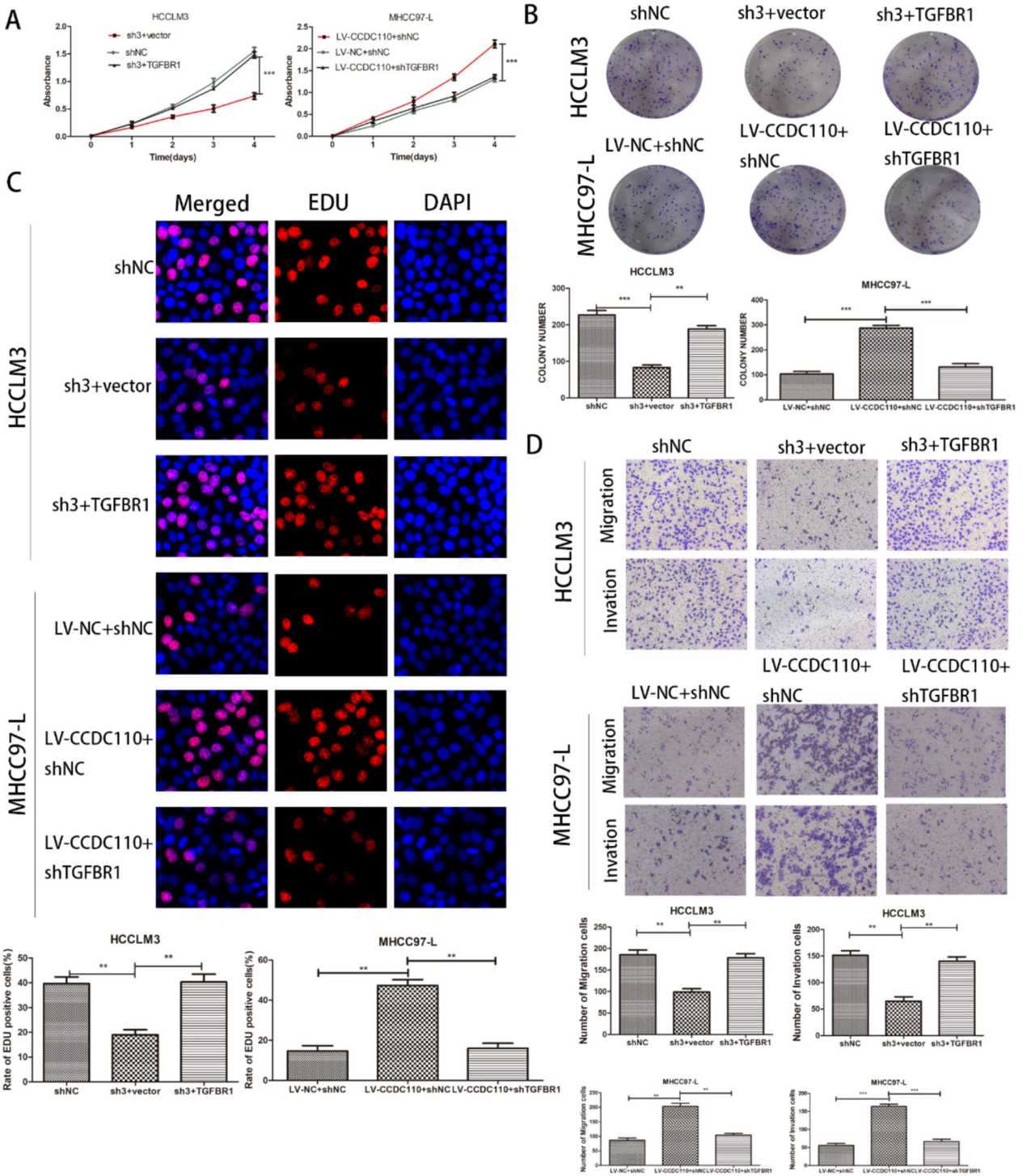

Fig. 5 The CCDC110-TGFBR1 axis promotes the malignant biological behavior of hepatocellular carcinoma cells in vitro. **A**–**C** CCK-8, colony formation, and EdU experiments verify that the cell proliferation inhibited by CCDC110 knockdown in HCCLM3 cells can be restored by overexpression of TGFBR1, and that the cell proliferation promoted by CCDC110 overexpression in MHCC97-L cells can be inhibited by knocking down TGFBR1 (Scale bar, 50 μm). **D** Migration and invasion experiments verify that cell migration and invasion inhibited by CCDC110 knockdown cannot be restored by overexpression of TGFBR1, and that cell migration and invasion promoted by CCDC110 overexpression cannot be inhibited by knocking down TGFBR1 (Scale bar, 50 μm). (***p < 0.001, **p < 0.01)

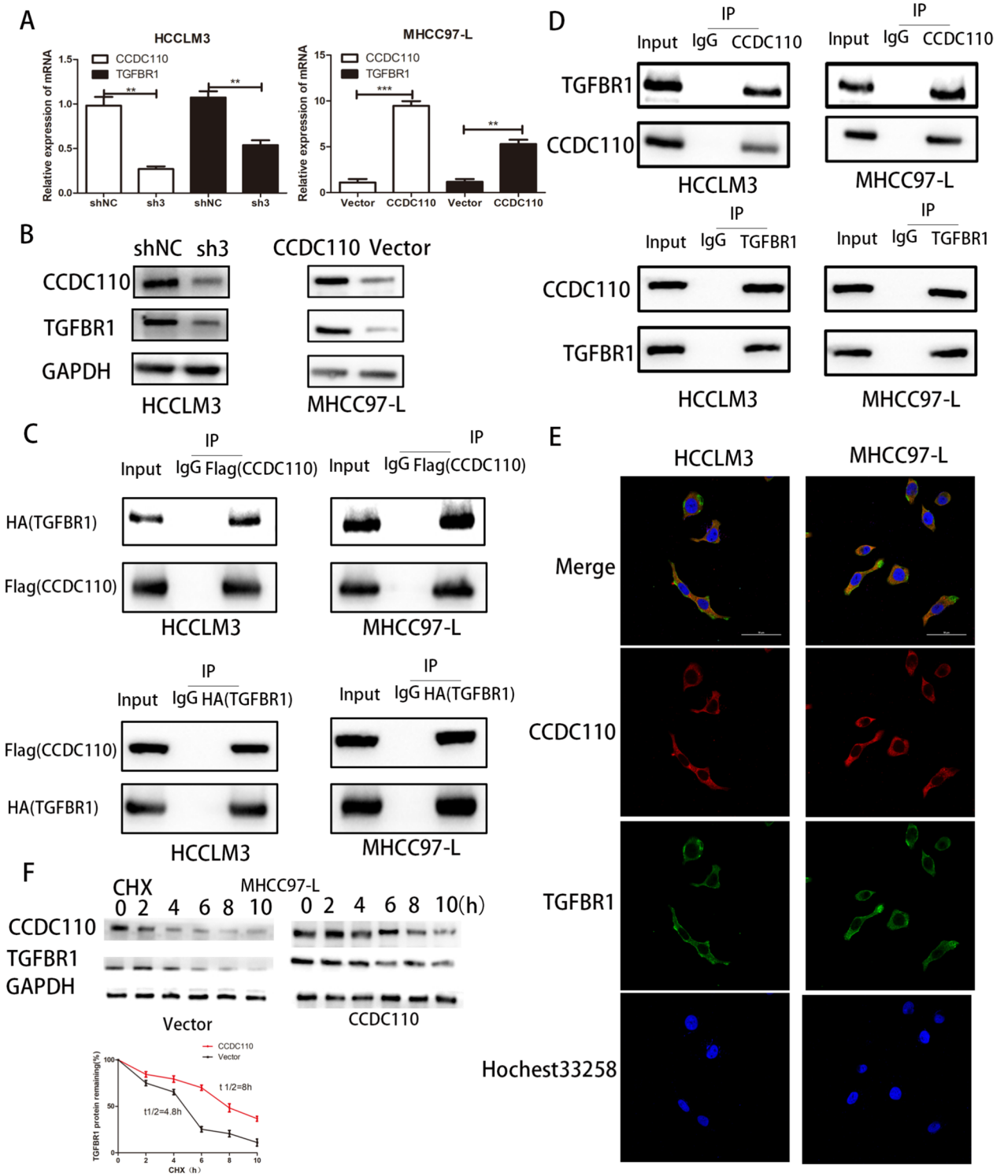

Fig. 6 The interaction and subcellular localization of CCDC110 and TGFBR1 in hepatocellular carcinoma cells. **A**, **B** qRT-PCR and Western blot experiments validate the expression of TGFBR1 in HCCLM3 cells with CCDC110 knockdown and in MHCC97-L cells with CCDC110 overexpression. **C** Exogenous immunoprecipitation experiments using Flag and HA antibodies. **D** Endogenous immunoprecipitation experiments using CCDC110 and TGFBR1 antibodies. **E** Subcellular localization of CCDC110 and TGFBR1 in HCCLM3 and MHCC97-L cells. **F** CCDC110 regulates the stability of TGFBR1. (***p < 0.001, **p < 0.01)

experiment to verify whether CCDC110 can affect the stability of TGFBR1. We found that as CHX treatment time increased, the decrease in TGFBR1 content in the CCDC110-overexpressing group decreased more slowly than that in the control group (Fig. 6F). The experimental findings indicated that the stability of TGFBR1 was significantly increased following the overexpression of CCDC110, suggesting that CCDC110 plays a role in maintaining TGFBR1 stability. In mammalian cells, the ubiquitin–proteasome system represents the primary mechanism for protease activity, facilitating protein degradation [47–49]. The ubiquitination process begins with the ubiquitin-activating enzyme (E1) and the ubiquitin-conjugating enzyme (E2), which prepare the ubiquitin ligase [50]. Subsequently, the ubiquitin ligase (E3) attaches ubiquitin to the target protein, thereby specifying the ubiquitin substrate [50]. Proteins marked with ubiquitin are then degraded by the 26S proteasome [51]. To this end, HCC cells were treated with the proteasome inhibitor MG132. The results demonstrated that CCDC110 knockdown reduced the protein expression of TGFBR1 in HCCLM3 cells, which was reversed by MG132 (Fig. 7A). Conversely, overexpression of CCDC110 increased TGFBR1 protein levels in MHCC97-L cells, an effect that was counteracted by MG132 (Fig. 7B). Further analysis of TGFBR1 ubiquitination levels under various conditions revealed that CCDC110 knockdown significantly increased TGFBR1 ubiquitination in HCCLM3 cells, whereas CCDC110 overexpression decreased TGFBR1 ubiquitination in MHCC97-L cells (Fig. 7C, D). In conclusion, these findings suggest that CCDC110 augments TGFBR1 protein levels in HCC cells by inhibiting ubiquitin/proteasome-dependent protein degradation.

Effect of the CCDC110-TGFBR1 axis on the apoptosis of hepatocellular carcinoma cells.

We overexpressed TGFBR1 in HCCLM3 cells with CCDC110 knockdown and knocked down TGFBR1 in MHCC97-L cells with CCDC110 overexpression. Flow cytometry was used to measure the percentage of apoptotic cells in each group. The results revealed that knocking down CCDC110 in HCCLM3 cells promoted cell apoptosis, but the percentage of apoptotic HCCLM3 cells decreased after TGFBR1 was overexpressed ($p < 0.01$) (Fig. 8A). The overexpression of CCDC110 in MHCC97-L cells inhibited cell apoptosis, but the percentage of apoptotic MHCC97-L cells increased after TGFBR1 was knocked down ($p < 0.01$) (Fig. 8B). Studies have shown that cell apoptosis is closely related to the antiapoptotic gene Bcl-2, the proapoptotic gene Bax, and caspase-3, PARP1. Western blot analysis demonstrated that silencing CCDC110 in HCCLM3 cells notably reduced the expression of Bcl-2, elevated the expression of Bax, and triggered caspase-3 and PARP1 cleavage, which significantly increased the expression of cleaved caspase-3 and cleaved PARP1. Conversely, TGFBR1 overexpression markedly increased the expression of Bcl-2, decreased the expression of Bax, and significantly reduced the expression of cleaved caspase-3 and cleaved PARP1, with caspase-3 and PARP1 expression remaining consistent across groups. Similarly, CCDC110 overexpression in MHCC97-L cells significantly increased the expression of Bcl-2, decreased the expression of Bax, and notably reduced the expression of cleaved caspase-3 and cleaved PARP1. On the other hand, TGFBR1 knockdown substantially reduced the expression of Bcl-2, increased the expression of Bax, and significantly elevated the expression of cleaved caspase-3 and cleaved PARP1, with no difference in caspase-3 and PARP1 expression observed between the groups ($p < 0.01$) (Fig. 8C, D). These findings suggest that the CCDC110-TGFBR1 axis might influence the apoptosis of hepatocellular carcinoma cells by modulating the balance between Bcl-2/Bax expression and the caspase-3 pathway Table 4.

The CCDC110-TGFBR1 axis promotes the proliferation and metastasis of hepatocellular carcinoma in vivo.

Similar to the in vitro experiments, we first used LV-CCDC110 to construct stable CCDC110-overexpressing MHCC97-L hepatocellular carcinoma cells. We subsequently used TGFBR1 shRNA to stably interfere with the expression of TGFBR1. We subsequently conducted subcutaneous tumor experiments on nude mice, and the results revealed that the size, quality, and growth rate of subcutaneous tumors in the stable CCDC110-overexpressing group were significantly greater than those in the control group ($p < 0.001$). However, after TGFBR1 was knocked down in CCDC110-overexpressing MHCC97-L cells, the enhanced tumorigenic ability induced by CCDC110 overexpression was again suppressed ($p < 0.01$), as shown in Fig. 9A–C. We performed immunohistochemical staining for a tumor proliferation biomarker (Ki67) and immunofluorescence staining for a tumor apoptosis biomarker (TUNEL) on subcutaneous tumor tissue slices. CCDC110 overexpression promoted tumor proliferation and inhibited apoptosis, and after TGFBR1 knockdown, tumor proliferation was suppressed, and apoptosis was promoted ($p < 0.05$), as shown in Fig. 9D, E. In an orthotopic liver tumor experiment in nude mice, we also reported that after CCDC110 overexpression, the volume of orthotopic tumors significantly increased. Subsequent to the knockdown of TGFBR1, there was a significant reduction in the volume of orthotopic tumors

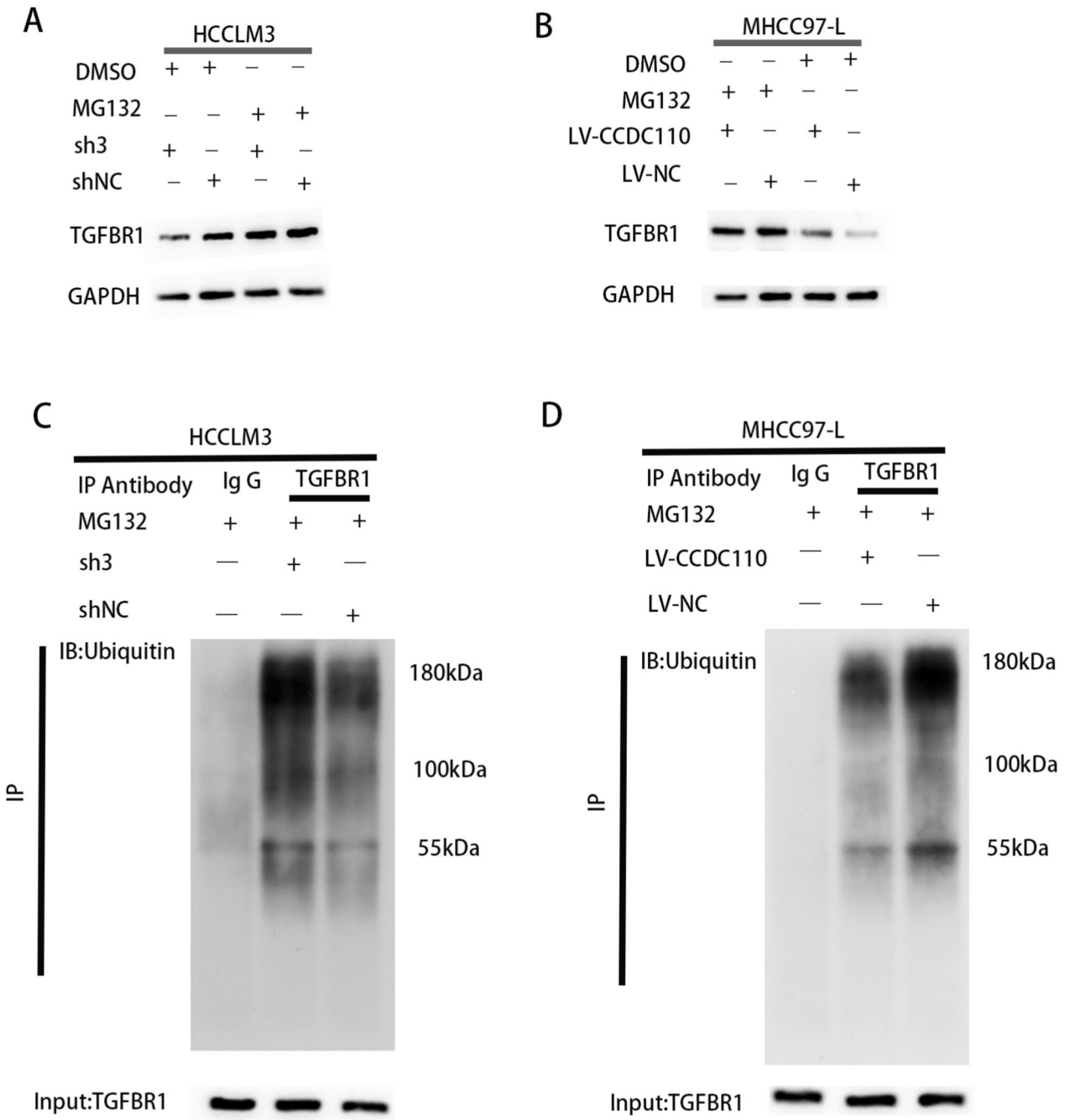

Fig. 7 CCDC110 accelerated ubiquitin/proteasome-dependent protein degradation of TGFBR1. **a**, **b** Protein level of TGFBR1 in HCC cells treated with 20 μM MG132 for 12 h. 10a, HCCLM3 cells transfected with CCDC110 shRNA and control; 10b, MHCC97-L cells transfected with lentivirus for CCDC110 overexpression and control. **c**, **d** Ubiquitination modification of TGFBR1 proteins in HCC cells was determined via Co-IP and western blotting

($p < 0.01$), as depicted in Fig. 9F. To ascertain whether the CCDC110-TGFBR1 axis facilitates the metastasis of hepatocellular carcinoma in vivo, a metastatic tumor model in nude mice was established. Following a 28-day period, the mice were euthanized, and their lungs were harvested and subjected to HE staining. The findings indicated that the number of lung nodules in the CCDC110-overexpressing group was significantly greater than that in the control group. Conversely, the number of lung nodules significantly

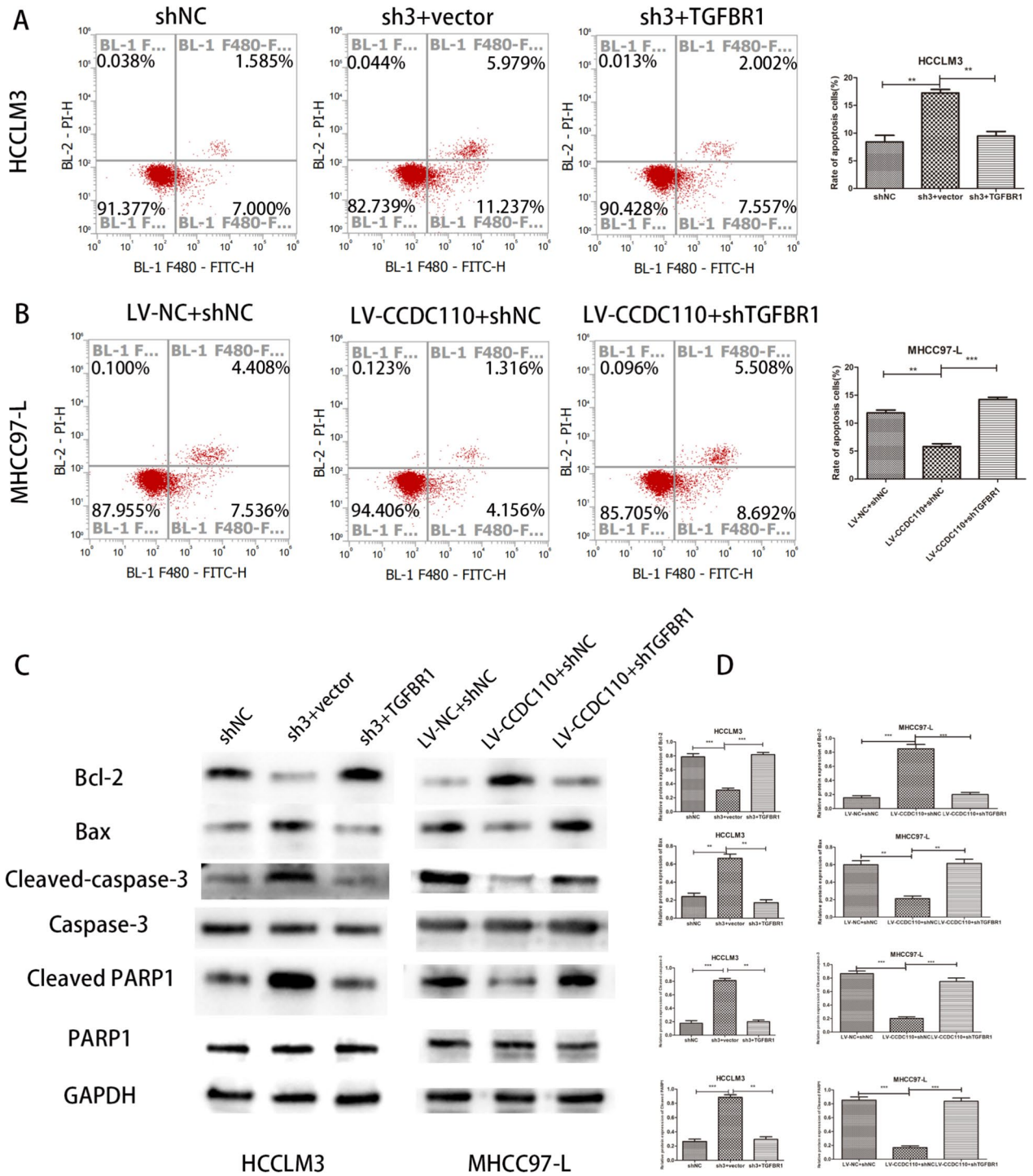

Fig. 8 The effect of the CCDC110-TGFBR1 axis on apoptosis in hepatocellular carcinoma cells. **A** Apoptosis experiment validation showed that the apoptosis ability of HCCLM3 cells promoted by CCDC110 knockdown could be restored by TGFBR1 overexpression. **B** Apoptosis experiment validation showed that the apoptosis ability of MHCC97-L cells inhibited by CCDC110 overexpression could be restored by TGFBR1 knockdown. **C**, **D**. Western blot experiment detected the protein expression levels of Bcl-2, Bax, Caspase-3, Cleaved Caspase-3, PARP1 and Cleaved PARP1 in each group. (***$p < 0.001$, **$p < 0.01$)

Table 4 PCR引物序列

	Forward primer	Reverse primer
CCDC110	GGATTTGCCTACAGAGAATCA	TGGGATGGAACATTTACACTT
GAPDH	CCTTCCGTGTCCCCACT	GCCTGCTTCACCACCTTC

decreased following TGFBR1 knockdown ($p < 0.001$), as illustrated in Fig. 9G. These observations suggest that CCDC110 can enhance the malignant biological behavior of hepatocellular carcinoma cells in vivo via TGFBR1.

The CCDC110-TGFBR1 axis activates the TGF-β/SMAD signaling pathway.

Previously established CCDC110-knockdown and CCDC110-overexpressing HCCLM3 and MHCC97-L hepatocellular carcinoma cell lines, respectively, were used for Western blot experiments to assess the protein expression levels of TGFBR1 and downstream Smad2 and Smad3 in both the knockdown and overexpression groups. These findings indicated that silencing CCDC110 resulted in a decrease in TGFBR1 protein expression and significantly decreased levels of phosphorylated Smad2 (p-Smad2) and Smad3 (p-Smad3) proteins, whereas total Smad2 and Smad3 protein expression levels remained unchanged. On the other hand, overexpression of CCDC110 led to an increase in TGFBR1 protein expression and a significant increase in the protein levels of p-Smad2 and p-Smad3, with no difference in the total Smad2 and Smad3 protein levels (Fig. 10A). Given the well-documented role of TGFBR1 as an oncogene in human cancers and its critical involvement in TGF-β-induced EMT and tumor progression, additional Western blot experiments were conducted to examine the protein expression levels of EMT-related markers in each group. The results demonstrated that knockdown of CCDC110 in the HCCLM3 hepatocellular carcinoma cell line significantly increased the protein expression of the epithelial marker E-cadherin and notably decreased the protein expression of the mesenchymal markers N-cadherin and vimentin, along with the protein expression of matrix metalloproteinase (MMP) 2 and MMP9. Conversely, overexpression of CCDC110 in the MHCC97-L hepatocellular carcinoma cell line significantly decreased the protein expression of E-cadherin but significantly increased the protein expression of N-cadherin, vimentin, MMP2, and MMP9. To determine whether the activation of the Smad2 and Smad3 proteins by CCDC110 depends on TGFBR1, a selective TGFBR1 inhibitor (SB431542) was used to suppress TGFBR1 expression. Western blot analyses revealed that in both the knockdown and control groups, the protein expression levels of TGFBR1, phosphorylated Smad2 (p-Smad2), and phosphorylated Smad3 (p-Smad3) were significantly decreased, whereas the expression of E-cadherin was significantly increased. Additionally, the protein expression levels of N-cadherin, vimentin, MMP2, and MMP9 were significantly reduced. Similarly, the protein expression levels of TGFBR1, p-Smad2, and p-Smad3 were significantly lower in MHCC97-L cells than in control cells treated with SB431542 to inhibit TGFBR1 expression. The expression level of E-cadherin was significantly increased, and the expression levels of N-cadherin, vimentin, MMP2, and MMP9 were significantly decreased (Fig. 10B). Notably, CCDC110 overexpression did not activate downstream Smad2 and Smad3 when TGFBR1 expression was inhibited by SB431542, indicating that CCDC110 influences the activation of the TGF-β/SMAD signaling pathway and EMT progression through the regulation of TGFBR1 expression.

Activated TGFBR1 engages transiently with Smad2,3 and phosphorylates its C-terminal Ser residue, after which phosphorylated Smad2,3 dissociates from TGFBR1 and forms a complex with Smad4, thereby modulating the expression of target genes [59]. Immunofluorescence experiments confirmed the activation of the TGF-β/SMAD signaling pathway across different groups, showing that CCDC110 knockdown in HCCLM3 cells reduced Smad2/3 expression in the nucleus, suggesting decreased nuclear translocation of Smad2/3. However, following TGFBR1 expression inhibition with SB431542, no significant change in Smad2/3 nuclear translocation was observed between the knockdown and control groups (Fig. 10C). In MHCC97-L cells, CCDC110 overexpression increased Smad2/3 nuclear expression, indicating increased nuclear translocation of Smad2/3. However, after TGFBR1 expression was inhibited with SB431542, no significant change in Smad2/3 nuclear translocation was noted between the overexpression and control groups (Fig. 10D). Furthermore, immunofluorescence experiments were used to assess the expression levels of E-cadherin and vimentin after CCDC110 knockdown or overexpression. The results revealed that CCDC110 knockdown in HCCLM3 cells increased E-cadherin expression and reduced vimentin expression. The inhibition of TGFBR1 expression with SB431542 continued to increase E-cadherin expression while decreasing vimentin expression (Fig. 10E). Conversely, CCDC110 overexpression in MHCC97-L cells decreased E-cadherin expression and elevated vimentin expression. When TGFBR1 expression was inhibited by SB431542, E-cadherin expression increased, and vimentin expression decreased, indicating that CCDC110 overexpression

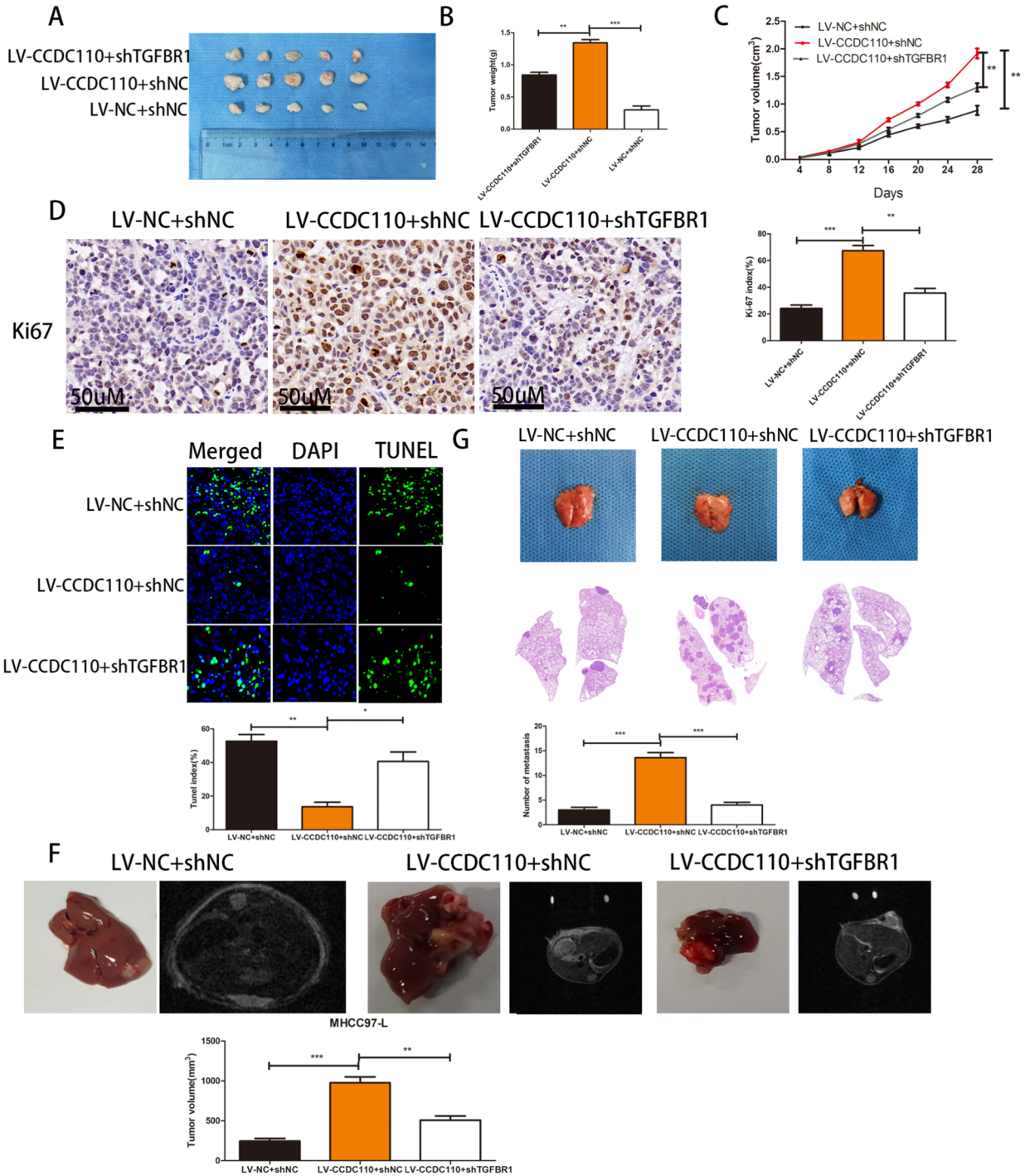

Fig. 9 The CCDC110-TGFBR1 axis promotes the progression of hepatocellular carcinoma in vivo. **A** Subcutaneous tumor experiments were conducted with three groups of hepatocellular carcinoma cells, LV-NC + shNC, LV-CCDC110 + shNC, and LV-CCDC110 + shTGFBR1, and the in vivo tumor formation was evaluated after 28 days. **B** The weight of subcutaneous tumors in each group. **C** The growth curve of subcutaneous tumors in each group. **D** The proliferation biomarker (Ki67) of subcutaneous tumor tissue slices was detected by immunohistochemistry (Scale bar: 50 μm). **E** The apoptosis biomarker (Tunel) of subcutaneous tumor tissue slices was detected by immunofluorescence staining. **F** Nude mice were injected with hepatocellular carcinoma cells via the tail vein to establish a lung metastasis model in LV-NC + shNC, LV-CCDC110 + shNC, and LV-CCDC110 + shTGFBR1 groups. After 28 days, the lungs were collected and the lung metastatic nodules were stained with HE. G. Orthotopic transplantation of xenograft tumors derived from MHCC97-L cells in nude mice was divided into three groups: LV-NC + shNC, LV-CCDC110 + shNC, and LV-CCDC110 + shTGFBR1. (***p < 0.001, **p < 0.01, *p < 0.05)

could not promote EMT in the presence of TGFBR1 inhibition by SB431542 (Fig. 10E). These findings align with previous Western blot results, collectively suggesting that the CCDC110-TGFBR1 axis drives EMT and the malignant behavior of hepatocellular carcinoma cells by activating the TGF-β/SMAD signaling pathway.

Analysis of the correlation between the CCDC110/TGFBR1 proteins in hepatocellular carcinoma tissue.

Previous studies have demonstrated that CCDC110 is highly expressed in hepatocellular carcinoma tissues, and the literature has reported high expression of TGFBR1 in such tissues [40]. CCDC110 and TGFBR1 interact and collectively enhance the proliferation, migration, and invasion of hepatocellular carcinoma cells within tumor tissues. Therefore, ten pairs of hepatocellular carcinoma tissue samples were randomly selected for immunohistochemical staining to observe the expression of CCDC110 and TGFBR1 in hepatocellular carcinoma tumor tissues and their corresponding normal tissues. The results indicated that both CCDC110 and TGFBR1 were expressed at higher levels in hepatocellular carcinoma tumor tissues than in paired normal tissues (Fig. 11A). Immunohistochemical staining scores further confirmed that the expression levels of CCDC110 and TGFBR1 in tumor tissues were significantly greater than those in paired normal tissues ($p < 0.001$) (Fig. 11B). Additionally, linear correlation analysis based on the immunohistochemical staining scores of CCDC110 and TGFBR1 in hepatocellular carcinoma tissues revealed a strong correlation between the expression of CCDC110 and TGFBR1 ($r = 0.6889$, $p < 0.05$) (Fig. 11C). Based on the expression levels of CCDC110 and TGFBR1 in 100 pairs of hepatocellular carcinoma tissues, patients were categorized into four groups: CCDC110 high/TGFBR1 high, CCDC110 high/TGFBR1 low, CCDC110 low/TGFBR1 high, and CCDC110 low/TGFBR1 low, and Kaplan–Meier survival analysis was performed. The analysis revealed that patients with co-high expression levels of CCDC110 and TGFBR1 had significantly poorer prognoses ($p < 0.001$, Hazard Ratio = 4.359, 95% CI of ratio:1.817 to 10.45) (Fig. 11D). Therefore, the expression of CCDC110 and TGFBR1 in hepatocellular carcinoma tissues is positively correlated, and combining the analysis of CCDC110 and TGFBR1 provides better prognostic guidance for patients with hepatocellular carcinoma than the analysis of CCDC110 alone.

Discussion

Hepatocellular carcinoma (HCC) represents the most prevalent form of primary liver cancer. Characterized by its rapid proliferation, invasive nature, and high metastatic potential, HCC continues to have a high mortality rate [2]. Surgical interventions, including liver transplantation and tumor resection, currently stand as the primary treatment options for HCC. However, most patients with HCC do not experience significant symptoms in the early stages of the disease and often miss the window for curative surgery at the time of diagnosis. Furthermore, the risk of recurrence or metastasis within five years post-surgery remains high, significantly affecting patient survival [52]. Investigating the mechanisms underlying HCC proliferation, invasion, and metastasis is crucial for identifying new biomarkers and offering fresh perspectives on early diagnosis and treatment strategies.

Coiled-coil domain-containing proteins (CCDCs) are versatile protein domains that form various spatial structures and exhibit a wide range of biological functions [15]. Numerous studies have shown that members of the CCDC family are aberrantly expressed in various cancer cells, including HCC cells, and play significant roles in the processes of tumor cell proliferation and metastasis [16–18]. As a CCDC family member, CCDC110 has been the subject of limited research regarding its biological functions and clinical significance in tumors, with only one study reporting elevated mRNA levels of CCDC110 in several cancers, such as tongue cancer, gastric cancer, melanoma, and HCC [26]. However, CCDC110 mRNA and protein expression levels in HCC tissues and cell lines have not been detected, and there has been no correlation analysis between CCDC110 expression and the clinical pathological features or prognosis of HCC patients.

Here, we demonstrated for the first time that CCDC110 is highly expressed in HCC tissues and cell lines. Elevated

(See figure on next page.)

Fig. 10 The CCDC110-TGFBR1 axis can activate the TGF-β/SMAD signaling pathway. **A** Western blot detects the expression of TGFBR1, smad2, smad3, p-smad2, p-smad3, E-cadherin, N-cadherin, vimentin, MMP-2, and MMP-9 in the knockdown and overexpression groups. **B** After adding SB431542 to inhibit TGFBR1 expression, western blot detects the expression of TGFBR1, p-smad2, p-smad3, E-cadherin, N-cadherin, vimentin, MMP-2, and MMP-9 in the knockdown and overexpression groups. **C** Immunofluorescence detection shows the subcellular localization of SMAD2 in the knockdown group, control group, and SB431542-treated group (Scale bar: 50 μm). **D** Immunofluorescence detection shows the subcellular localization of SMAD2 in the overexpression group, control group, and SB431542-treated group (Scale bar: 50 μm). **E** Immunofluorescence detection shows the expression of epithelial marker E-cadherin and mesenchymal marker vimentin in the knockdown, overexpression, and SB431542-treated groups (Scale bar: 50 μm)

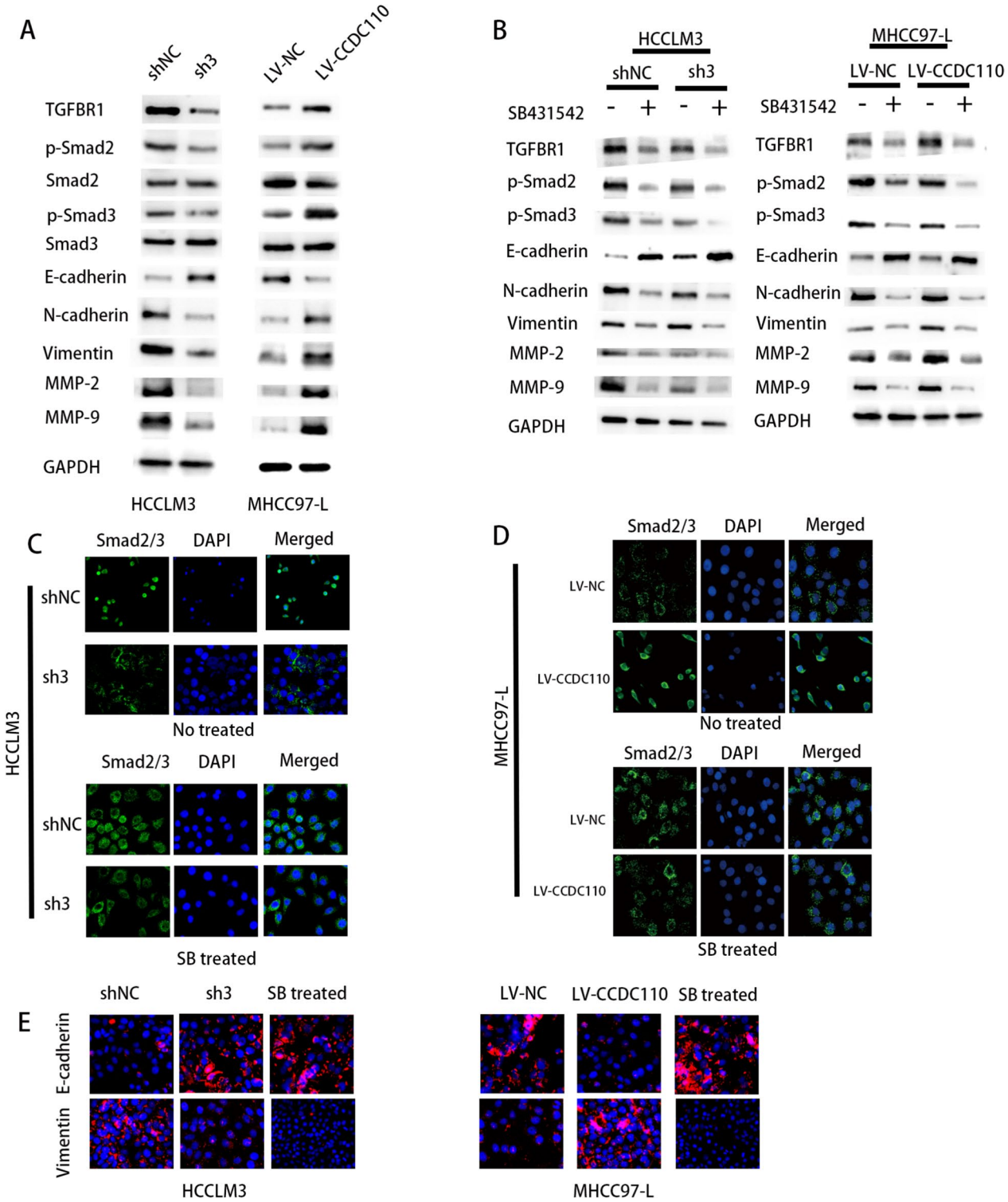

Fig. 10 (See legend on previous page.)

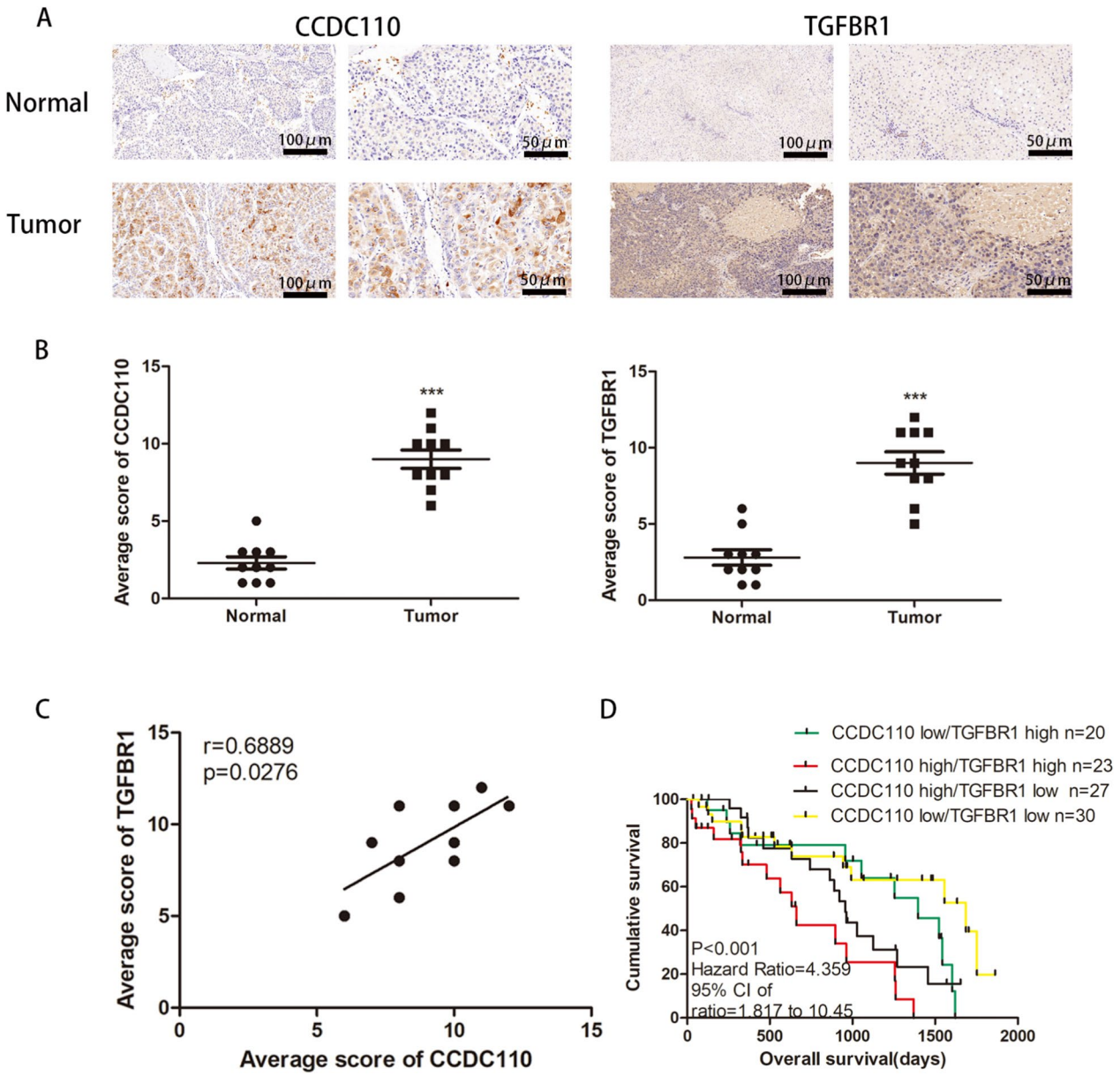

Fig. 11 The correlation between CCDC110 and TGFBR1 in hepatocellular carcinoma tissue, as well as the clinical prognosis analysis of CCDC110 and TGFBR1 combination. **A** Representative images of immunohistochemical staining of CCDC110 and TGFBR1 in tumor tissue and normal tissue paired with 10 hepatocellular carcinoma patients (Scale bar: 100 μm, 50 μm). **B** Scoring of immunohistochemical staining of CCDC110 and TGFBR1 in tumor tissue and normal tissue paired with 10 hepatocellular carcinoma patients. **C** Linear correlation analysis of CCDC110 and TGFBR1 expression in tumor tissue and normal tissue paired with 10 hepatocellular carcinoma patients. **D** Kaplan–Meier analysis showed the overall survival of 100 hepatocellular carcinoma patients with different expression levels of CCDC110 and TGFBR1. (***p < 0.001, **p < 0.01, *p < 0.05)

expression of CCDC110 results in the suppression of ubiquitin-mediated degradation of TGFBR1, subsequently activating the TGF-β/SMAD signaling pathway, which contributes to the initiation and progression of hepatocellular carcinoma (HCC).

In this investigation, transcriptome sequencing of HCC tissue samples was employed to identify differentially expressed genes. After those genes previously reported were eliminated, CCDC110 was chosen for further research. Early validation of the biological functions and clinical importance of CCDC110 in HCC led to the

identification of TGFBR1 as a target protein of CCDC110 via TMT-based quantitative proteomics. Located on chromosome 9q22.33 and spanning about 56 kb, TGFBR1 is a well-researched oncogene in human cancers and is known to play a pivotal role in TGF-β-induced EMT and tumor progression [32, 53]. Research has indicated that TGFBR1 mRNA expression levels are elevated in HCC and correlate with the TNM stage of HCC patients [42]. Furthermore, studies have shown that the overexpression of miR-4458 in HCC cell lines can inhibit tumor progression by targeting TGFBR1 [54]. Western blot experiments confirmed that TGFBR1 expression was decreased in HCC cell lines following CCDC110 knockdown and increased in cell lines with CCDC110 overexpression, which aligns with the TMT quantitative proteomics findings. Through immunoprecipitation and immunofluorescence experiments, the interaction between CCDC110 and TGFBR1 in HCC cells was validated. Proteins are essential for maintaining life activities, supporting normal metabolism, and facilitating substance transport, often functioning through complex formation with other proteins [55]. Protein–protein interactions are integral to cellular processes, including cell proliferation, death, and differentiation, and are pivotal in regulating cell signal transduction [56]. These interactions can enhance the dynamic features of intracellular proteins, altering substrate specificity and catalytic activity and regulating gene expression. Abnormalities in protein interactions can lead to various diseases, including cancer, positioning protein–protein interactions as potential targets for cancer therapy [57, 58].

Protein stability assays revealed that CCDC110 enhances the stability of the TGFBR1 protein. As a result, overexpression of CCDC110 leads to an increase in TGFBR1 protein expression. Previous studies have shown that TGFBR1 protein levels are regulated primarily via internalization and ubiquitination-mediated degradation. In this study, the binding of CCDC110 to TGFBR1 impeded its degradation and preserved its stability, possibly because the interaction of CCDC110 affects the ubiquitin recognition of TGFBR1, thus increasing its protein stability. Further in vivo and in vitro functional assays were conducted to confirm that CCDC110, through its interaction with TGFBR1, exacerbates the malignant biological behavior of hepatocellular carcinoma cells.

TGFBR1, a serine/threonine protein kinase receptor, plays a vital role in the TGF-β/SMAD signaling pathway and significantly impacts cancer progression through its regulation of cell growth, differentiation, and migration [40, 53]. The TGF-β signaling pathway, which is capable of acting as both a tumor promoter and a tumor suppressor depending on the tumor development stage, can induce EMT to facilitate cell invasion and metastasis [34, 35]. Once activated, TGFBR1 relays the TGF-β signal from the cell surface to the cytoplasm, phosphorylating Smad2 and Smad3 and forming a complex with Smad4 that moves to the nucleus to influence downstream gene transcription [59]. Abnormal TGFBR1 expression can disrupt the TGF-β signaling pathway, encouraging tumor development [40, 60]. Elevated TGFBR1 expression in hepatocellular carcinoma tissues has been linked to tumor progression inhibition upon TGFBR1 downregulation [42]. Additionally, TGFBR1 downregulation has been associated with reduced proliferation in lung cancer cells and decreased migration and invasion in breast cancer cells [61, 62]. Matrix metalloproteinases (MMPs), zinc-dependent endopeptidases, degrade various extracellular matrix proteins, including collagen and elastin, playing pivotal roles in processes such as cell proliferation, migration, differentiation, angiogenesis, tissue repair, and apoptosis inhibition. Specifically, MMP-2 and MMP-9 are crucial for extracellular matrix degradation, facilitating tumor invasion and metastasis. This study confirmed that alterations in CCDC110 expression impact the activation of the TGF-β/SMAD signaling pathway, triggering EMT in hepatocellular carcinoma and promoting tumor cell proliferation, invasion, and metastasis. SB431542, a synthetic molecule, inhibits TGFBR1 by binding to its ATP-binding site, preventing Smad2 and Smad3 phosphorylation [63]. Experiments with SB431542 in hepatocellular carcinoma cells demonstrated that the activation of the TGF-β/SMAD signaling pathway by CCDC110 and the induction of EMT depend on TGFBR1. A combined analysis of CCDC110/TGFBR1 expression in hepatocellular carcinoma tissues indicated superior prognostic prediction over single-factor analysis of CCDC110. These findings suggest that the CCDC110-TGFBR1 axis may serve as a novel therapeutic target for hepatocellular carcinoma.

Conclusion

This study revealed that both the mRNA and protein levels of CCDC110 are markedly elevated in hepatocellular carcinoma tissues and cell lines, which correlates with adverse prognostic outcomes for patients with hepatocellular carcinoma. CCDC110 expression is significantly positively associated with critical clinical parameters of hepatocellular carcinoma, such as tumor size, quantity, capsule integrity, microvascular invasion, Edmonson staging, and TNM staging. Functionally, CCDC110 facilitates the proliferation of hepatocellular carcinoma cells, reduces their degree of apoptosis, and enhances their

migration and invasion capabilities. At the molecular level, CCDC110 interacts with TGFBR1 within the cytoplasm, contributing to the increased stability of TGFBR1 by preventing its ubiquitination. Through TGFBR1, CCDC110 increases proliferation, inhibits apoptosis, and augments the migration and invasion of hepatocellular carcinoma cells both in vitro and in vivo. The synergy between CCDC110 and TGFBR1 promotes EMT, thereby enhancing the malignant biological behavior of hepatocellular carcinoma through the activation of the TGF-β/SMAD signaling pathway. Additionally, the protein expression levels of CCDC110 and TGFBR1 in hepatocellular carcinoma tissues are highly elevated and positively correlated. A combined analysis of CCDC110 and TGFBR1 offers enhanced prognostic value for patients with hepatocellular carcinoma, suggesting that the CCDC110-TGFBR1 axis is a potential target for therapeutic intervention in hepatocellular carcinoma.

Abbreviations

HCC	Hepatocellular carcinoma
CCDC110	Coiled-coil domain-containing 110
TMT	Tandem Mass Tags
TGFBR1	Transforming growth factor beta receptor 1
TCGA	The Cancer Genome Atlas
qRT-PCR	Quantitative reverse transcription PCR
IHC	Immunohistochemistry
WB	Western blot
Co-IP	Co-inmunoprecipitation
CHX	Cycloheximide
EMT	Epithelial-Mesenchymal Transition
TGF-β	Transforming growth factor beta
Smad2	SMAD family member 2
Smad3	SMAD family member 3
PBS	Phosphate Buffered Saline
PMSF	Phenylmethanesulfonyl fluoride
TBS	Tris buffered saline
ECL	Enhanced chemiluminescence
CCK-8	Cell Counting Kit-8
EdU	5-Ethynyl-2′-deoxyuridine
BSA	Bovine Serum Albumin
TBST	Tris-Buffered Saline with Tween-20
DEPC	Diethypyrocarbonate
DAB	3,3′-Diaminobenzidine
IF	Immunofluorescence
SDS-PAGE	Sodium dodecyl sulfate–polyacrylamide gel
MRI	Magnetic resonance imaging
shRNA	Short hairpin RNA
BCA	Bicinchoninic acid
MMP	Matrix metalloproteinase
HE	Hematoxylin and eosin staining
OD	Opital density
FBS	Fetal bovine serum
HRP	Horseradish peroxidase
APS	Ammonium persulfate
SDS	Sodium dodecyl sulfate
IgG	Immunoglobulin G
Tris	N-trishydroxymethyl aminomethane
TME	Tumor microenvironment
ECM	Extracellular matrix
HSC	Hepatic stellate cells
CAF	Cancer-associated fibroblasts

Supplementary Information

The online version contains supplementary material available at https://doi.org/10.1186/s12935-025-03803-0.

Additional file 1: Figure S1. Transcriptome sequencing analysis of hepatocellular carcinoma tissue. A. Analysis of differentially expressed genes between 6 pairs of hepatocellular carcinoma tissues and their paired normal tissues ($p<0.05$, log2FoldChange>1). B. Heatmap analysis of the top 9 genes with the most significant differences among the upregulated 1019 genes. Figure S2. Detection of the transfection efficiency of CCDC110. A-B. The interference efficiency of CCDC110 in HCCLM3 and YY8103 cell lines was verified by qRT-PCR; C-D. the overexpression efficiency of CCDC110 in MHCC97-L and Huh7 cell lines was verified by qRT-PCR. (***$p<0.001$, **$p<0.01$). Figure S3. Functional recovery experiments of downstream target proteins of CCDC110. A. Western blot experiment validates the expression levels of RO60, ELMOD2, WNT5A, TGFBR1, and FNBP1L in HCCLM3 cells with CCDC110 knockdown. B-C. CCK-8 and EdU experiments verify that cell proliferation inhibited by CCDC110 knockdown cannot be restored by overexpression of RO60 or WNT5A (Scale bar, 100 μm). D. Migration and invasion experiments verify that cell migration and invasion inhibited by CCDC110 knockdown cannot be restored by overexpression of RO60 or WNT5A (Scale bar, 50 μm). (***$p<0.001$, **$p<0.01$). Figure S4. Functional recovery experiments of downstream target proteins of CCDC110. A. Western blot experiment validates the expression levels of RO60, ELMOD2, WNT5A, TGFBR1, and FNBP1L in MHCC97-L cells with CCDC110 overexpression. B-C. CCK-8 and EdU experiments verify that the cell proliferation promoted by CCDC110 overexpression cannot be inhibited by knocking down RO60 or WNT5A (Scale bar, 100 μm). D. Migration and invasion experiments verify that cell migration and invasion enhanced by CCDC110 overexpression cannot be inhibited by knocking down RO60 or WNT5A (Scale bar, 50 μm). (***$p<0.001$, **$p<0.01$)

Acknowledgements
We acknowledge TCGA database for providing public platforms, and the researchers for uploading their data. We acknowledge the Public Scientific Research Platform of Affiliated Zhongda Hospital of Southeast University for technical assistance.

Author contributions
Hao Shen designed the experiment. Hao Shen, Haifeng Li and Haodong Tang performed the experiments and data analysis. Hao Shen wrote and reviewed the manuscript. All authors have read and approved the final manuscript.

Funding
This work was supported by grants from the National Natural Science Foundation of China (82027806, 81572408).

Availability of data and materials
Please contact the corresponding author for data requests. No datasets were generated or analysed during the current study.

Declarations

Ethics approval and consent to participate
This study was approved by the Medical Ethics Committee of Affiliated Zhongda Hospital of Southeast University.

Competing interests
The authors declare that they have no competing interests.

Received: 14 August 2024 Accepted: 1 May 2025
Published online: 20 May 2025

References

1. Llovet JM, Kelley RK, Villanueva A, et al. Hepatocellular carcinoma. Nat Rev Dis Primers. 2021;7(1):6.
2. Sung H, Ferlay J, Siegel RL, et al. Global cancer statistics 2020 GLOBOCAN estimates of incidence and mortality worldwide for 36 cancers in 185 countries. CA. 2021;71(3):209–49.
3. Cao W, Chen HD, Yu YW, et al. Changing profiles of cancer burden worldwide and in China: a secondary analysis of the global cancer statistics 2020. Chin Med J. 2021;134(7):783–91.
4. Xia C, Dong X, Li H, et al. Cancer statistics in China and United States, 2022: profiles, trends, and determinants. Chin Med J. 2022;135(5):584–90.
5. Chen W, Zheng R, Baade PD, et al. Cancer statistics in China, 2015. Case. 2016;66(2):115–32.
6. Péneau C, Imbeaud S, La Bella T, et al. Hepatitis B virus integrations promote local and distant oncogenic driver alterations in hepatocellular carcinoma. Gut. 2022;71(3):616–26.
7. El-Serag HB. Epidemiology of viral hepatitis and hepatocellular carcinoma. Gastroenterology. 2012;142(6):1264-1273.e1261.
8. Younossi ZM, Koenig AB, Abdelatif D, et al. Global epidemiology of nonalcoholic fatty liver disease-Meta-analytic assessment of prevalence, incidence, and outcomes. Hepatology MD). 2016;64(1):73–84.
9. Yang JD, Hainaut P, Gores GJ, et al. A global view of hepatocellular carcinoma: trends, risk, prevention and management. Nat Rev Gastroenterol Hepatol. 2019;16(10):589–604.
10. Njei B, Rotman Y, Ditah I, et al. Emerging trends in hepatocellular carcinoma incidence and mortality. Hepatology. 2015;61(1):191–9.
11. Vibert E, Schwartz M, Olthoff KM. Advances in resection and transplantation for hepatocellular carcinoma. J Hepatol. 2020;72(2):262–76.
12. Apostolovic B, Danial M, Klok HA. Coiled coils: attractive protein folding motifs for the fabrication of self-assembled, responsive and bioactive materials. Chem Soc Rev. 2010;39(9):3541–75.
13. Rose A, Schraegle SJ, Stahlberg EA, et al. Coiled-coil protein composition of 22 proteomes–differences and common themes in subcellular infrastructure and traffic control. BMC Evol Biol. 2005;5:66.
14. Lupas AN, Bassler J, Dunin-Horkawicz S. The structure and topology of α-helical coiled coils. Subcell Biochem. 2017;82:95–129.
15. Truebestein L, Leonard TA. Coiled-coils: the long and short of it. BioEssays. 2016;38(9):903–16.
16. Gong Y, Qiu W, Ning X, et al. CCDC34 is up-regulated in bladder cancer and regulates bladder cancer cell proliferation, apoptosis and migration. Oncotarget. 2015;6(28):25856–67.
17. Tanouchi A, Taniuchi K, Furihata M, et al. CCDC88A, a prognostic factor for human pancreatic cancers, promotes the motility and invasiveness of pancreatic cancer cells. J Exper Clin Cancer Res. 2016;35(1):190.
18. Yin DT, Xu J, Lei M, et al. Characterization of the novel tumor-suppressor gene CCDC67 in papillary thyroid carcinoma. Oncotarget. 2016;7(5):5830–41.
19. Park SJ, Jang HR, Kim M, et al. Epigenetic alteration of CCDC67 and its tumor suppressor function in gastric cancer. Carcinogenesis. 2012;33(8):1494–501.
20. Wang J, Wu X, Dai W, et al. The CCDC43-ADRM1 axis regulated by YY1, promotes proliferation and metastasis of gastric cancer. Cancer Lett. 2020;482:90–101.
21. Wang J, Liu G, Liu M, et al. The FOXK1-CCDC43 axis promotes the invasion and metastasis of colorectal cancer cells. Cell Physiol Biochem. 2018;51(6):2547–63.
22. Farfsing A, Engel F, Seiffert M, et al. Gene knockdown studies revealed CCDC50 as a candidate gene in mantle cell lymphoma and chronic lymphocytic leukemia. Leukemia. 2009;23(11):2018–26.
23. Chen M, Ni J, Chang HC, et al. CCDC62/ERAP75 functions as a coactivator to enhance estrogen receptor beta-mediated transactivation and target gene expression in prostate cancer cells. Carcinogenesis. 2009;30(5):841–50.
24. Ning Y, Wang C, Liu X, et al. CK2-mediated CCDC106 phosphorylation is required for p53 degradation in cancer progression. J Exp Clin Cancer Res. 2019;38(1):131.
25. Zhang X, Zheng Q, Wang C, et al. CCDC106 promotes non-small cell lung cancer cell proliferation. Oncotarget. 2017;8(16):26662–70.
26. Monji M, Nakatsura T, Senju S, et al. Identification of a novel human cancer/testis antigen, KM-HN-1, recognized by cellular and humoral immune responses. Clin Cancer Res. 2004;10(18 Pt 1):6047–57.
27. Lee SN, Hong KM, Seong YS, et al. Ectopic overexpression of coiled-coil domain containing 110 delays G2/M entry in U2-OS cells. Develop Reproduct. 2020;24(2):101–11.
28. Chen YT, Scanlan MJ, Sahin U, et al. A testicular antigen aberrantly expressed in human cancers detected by autologous antibody screening. Proc Natl Acad Sci USA. 1997;94(5):1914–8.
29. Scanlan MJ, Gure AO, Jungbluth AA, et al. Cancer/testis antigens: an expanding family of targets for cancer immunotherapy. Immunol Rev. 2002;188:22–32.
30. Vaughan HA, St Clair F, Scanlan MJ, et al. The humoral immune response to head and neck cancer antigens as defined by the serological analysis of tumor antigens by recombinant cDNA expression cloning. Cancer Immun. 2004;4:5.
31. Park HJ, Seo HJ, Kim HW, et al. The centrosomal localization of KM-HN-1 (MGC33607) depends on the leucine zipper motif and the C-terminal coiled-coil domain. Exp Mol Med. 2007;39(6):828–38.
32. Wang J, Xiang H, Lu Y, et al. Role and clinical significance of TGF-β1 and TGF-βR1 in malignant tumors (Review). Int J Mol Med. 2021;47(4):55.
33. Syed V. TGF-β Signaling in Cancer. J Cell Biochem. 2016;117(6):1279–87.
34. Hao Y, Baker D, Ten Dijke P. TGF-β-mediated epithelial-mesenchymal transition and cancer metastasis. Int J Mol Sci. 2019;20(11):2767.
35. Wang S, Tong X, Li C, et al. Quaking 5 suppresses TGF-β-induced EMT and cell invasion in lung adenocarcinoma. EMBO Rep. 2021;22(6): e52079.
36. Hata A, Chen YG. TGF-β Signaling from receptors to Smads. Cold Spring Harb Perspect Biol. 2016;8(9): a022061.
37. Tzavlaki K, Moustakas A. TGF-β signaling. Biomolecules. 2020;10(3):487.
38. Guan L, Zhang L, Wang T, et al. POM121 promotes proliferation and metastasis in non-small-cell lung cancer through TGF-β/SMAD and PI3K/AKT pathways. Cancer Biomark. 2021;32(3):293–302.
39. Yu Y, Feng XH. TGF-β signaling in cell fate control and cancer. Curr Opin Cell Biol. 2019;61:56–63.
40. Kwon W, Choi SK, Kim D, et al. ZNF507 affects TGF-β signaling via TGFBR1 and MAP3K8 activation in the progression of prostate cancer to an aggressive state. J Experim Clin Cancer Res. 2021;40(1):291.
41. Yin H, Chen L, Piao S, et al. M6A RNA methylation-mediated RMRP stability renders proliferation and progression of non-small cell lung cancer through regulating TGFBR1/SMAD2/SMAD3 pathway. Cell Death Differentiat. 2021;30:605–17.
42. Tang YH, He GL, Huang SZ, et al. The long noncoding RNA AK002107 negatively modulates miR-140-5p and targets TGFBR1 to induce epithelial-mesenchymal transition in hepatocellular carcinoma. Mol Oncol. 2019;13(5):1296–310.
43. Dou W, Yang M, Su Y, et al. Dysregulation of miR-3607 predicts prognosis of hepatocellular carcinoma and regulates tumor cell proliferation, migration and invasion. Diagn Pathol. 2020;15(1):54.
44. Wang T, Yang N, Liang C, et al. Detecting protein-protein interaction based on protein fragment complementation assay. Curr Protein Pept Sci. 2020;21(6):598–610.
45. De Las RJ, Alonso-López D, Arroyo MM. Human interactomics: comparative analysis of different protein interaction resources and construction of a cancer protein-drug bipartite network. Adv Protein Chem Struct Biol. 2018;111:263–82.
46. Ivanov AA, Revennaugh B, Rusnak L, et al. The OncoPPi Portal: an integrative resource to explore and prioritize protein-protein interactions for cancer target discovery. Bioinformatics. 2018;34(7):1183–91.
47. Sharma A, Khan H, Singh TG, Grewal AK, Najda A, Kawecka-Radomska M, et al. Pharmacological modulation of ubiquitin-proteasome pathways in oncogenic signaling. Int J Mol Sci. 2021;22:11971.
48. Toma-Fukai S, Shimizu T. Structural diversity of ubiquitin E3 ligase. Molecules. 2021;26:6682.
49. Varshavsky A. The ubiquitin system, autophagy, and regulated protein degradation. Annu Rev Biochem. 2017;86:123–8.
50. Stewart MD, Ritterhoff T, Klevit RE, Brzovic PS. E2 enzymes: more than just middle men. Cell Res. 2016;26:423–40.
51. Rousseau A, Bertolotti A. Regulation of proteasome assembly and activity in health and disease. Nat Rev Mol Cell Biol. 2018;19:697–712.
52. Wang Z, Zhang G, Wu J, et al. Adjuvant therapy for hepatocellular carcinoma: current situation and prospect. Drug Discover Therapeut. 2013;7(4):137–43.

53. Pasche B, Pennison MJ, Jimenez H, et al. TGFBR1 and cancer susceptibility. Trans Am Clin Climatol Assoc. 2014;125:300–12.
54. Zhang Y, Shi K, Liu H, et al. miR-4458 inhibits the epithelial-mesenchymal transition of hepatocellular carcinoma cells by suppressing the TGF-β signaling pathway via targeting TGFBR1. Acta Biochim Biophys Sin. 2020;52(5):554–62.
55. Berggård T, Linse S, James P. Methods for the detection and analysis of protein-protein interactions. Proteomics. 2007;7(16):2833–42.
56. Braun P, Gingras AC. History of protein-protein interactions: from egg-white to complex networks. Proteomics. 2012;12(10):1478–98.
57. Rabbani G, Baig MH, Ahmad K, et al. Protein-protein interactions and their role in various diseases and their prediction techniques. Curr Protein Pept Sci. 2018;19(10):948–57.
58. Dar KB, Bhat AH, Amin S, et al. Exploring proteomic drug targets, therapeutic strategies and protein-protein interactions in cancer: mechanistic view. Curr Cancer Drug Targets. 2019;19(6):430–48.
59. Hata A, Chen YG. TGF-β signaling from receptors to smads. Cold Spring Harbor Perspect Bio. 2016;8(9):a022061.
60. Wang H, Zhang Q, Wang B, et al. miR-22 regulates C2C12 myoblast proliferation and differentiation by targeting TGFBR1. Eur J Cell Biol. 2018;97(4):257–68.
61. Moore-Smith L, Pasche B. TGFBR1 signaling and breast cancer. J Mammary Gland Biol Neoplasia. 2011;16(2):89–95.
62. Gao P, Wang H, Yu J, et al. miR-3607-3p suppresses non-small cell lung cancer (NSCLC) by targeting TGFBR1 and CCNE2. PLoS Genet. 2018;14(12): e1007790.
63. Ishigami I, Shuwari N, Kaminade T, et al. A TGFβ signaling inhibitor, SB431542, inhibits reovirus-mediated lysis of human hepatocellular carcinoma cells in a TGFβ-independent manner. Anticancer Res. 2021;41(5):2431–40.

Publisher's Note

Springer Nature remains neutral with regard to jurisdictional claims in published maps and institutional affiliations.